JGR Oceans

RESEARCH ARTICLE
10.1029/2022JC018987

Heat Transport by Mesoscale Eddies in the Norwegian and Greenland Seas

I. L. Bashmachnikov[1,2,3], R. P. Raj[4,5], P. Golubkin[1], and I. E. Kozlov[3]

[1]Nansen International Environmental and Remote Sensing Centre, Saint-Petersburg, Russia, [2]Department of Oceanography, Saint-Petersburg State University, Saint-Petersburg, Russia, [3]Marine Hydrophysical Institute of RAS, Sevastopol, Russia, [4]Nansen Environmental and Remote Sensing Centre, Bergen, Norway, [5]Bjerknes Center for Climate Research, Bergen, Norway

Abstract Ocean vortices are an important regional agent of water transport and cross-frontal exchange. This study is a first attempt to compare statistics of 3D properties of mesoscale eddies over the Norwegian and Greenland Seas. Results suggest that eddies in the central Greenland Sea are less intense, have smaller vertical extent and much smaller heat anomalies in their cores compared to eddies in the Lofoten Basin of the Norwegian Sea. In addition, these results suggest a relatively small inter-basin eddy exchange. The large-scale pattern of eddy translations shows that eddies cyclonically skirt the Norwegian-Greenland region. There is also a regional cyclonic pattern in the Lofoten Basin with a consistent signature of eddy merger in the northern part of the basin. We confirm that eddies generated from the Norwegian Atlantic Slope Current (NwASC) have a significant effect on the amount of heat the NwASC brings to the Arctic. The heat lost from the NwASC between the Svinoy and Sorkapp sections associated with the westward eddy heat transport translates to 70 ± 23 TW, 90% of which occurs in the Lofoten Basin. This accounts to 35% of the heat advected by the NwASC across the Svinoy section and is comparable with the heat loss in the Barents Sea. Interannual variability of the heat flux due to a change in the number of generated eddies is relatively small (∼10 TW). Nevertheless, our estimates suggest that, by varying temperature of their cores, the generated eddies can effectively damp temperature anomalies that propagate north along the NwASC.

Plain Language Summary Mesoscale eddies in the ocean are large rotating water bodies with typical radii between 10 and 100 km and vertical extents of a few hundred meters. These eddies can be an important regional agent of water transport and cross-frontal exchange. In this study we found that eddies in the Norwegian Sea have notably larger vertical extent, rotating velocity and intensity of thermohaline anomalies in their cores compared to those in the Greenland Sea. This suggests the predominantly local origin of eddies in each of the basins and a small inter-basin exchange. All eddies move counterclockwise around the Norwegian-Greenland region. Counterclockwise eddy translations are also registered in the Lofoten Basin. Propagating away from their generation regions (the continental margin of Lofoten Islands and western Spitsbergen) eddies merge and, on average, become bigger. In the Norwegian Sea, eddies extract about 70 TW of heat from the Norwegian Atlantic Slope Current, which reduces the northward heat transport of the current by one third and is comparable with the amount of heat extracted into the Barens. This eddy heat transport can effectively damp water temperature anomalies propagating along the current from the mid-latitudes North Atlantic into the Arctic.

Key Points:

- Eddies in the Greenland and Norwegian Seas show clear differences in intensity of thermohaline and dynamic anomalies of their cores
- The westward eddy heat transport accounts for about one third of heat loss from the Norwegian Atlantic Slope Current (NwASC)
- Eddy heat flux can effectively damp temperature anomalies as they propagate north along the NwASC

Correspondence to:
I. L. Bashmachnikov,
igorb@niersc.spb.ru

Citation:
Bashmachnikov, I. L., Raj, R. P., Golubkin, P., & Kozlov, I. E. (2023). Heat Transport by mesoscale eddies in the Norwegian and Greenland Seas. *Journal of Geophysical Research: Oceans*, *128*, e2022JC018987. https://doi.org/10.1029/2022JC018987

Received 15 JUN 2022
Accepted 2 FEB 2023

Author Contributions:
Conceptualization: I. L. Bashmachnikov
Data curation: I. L. Bashmachnikov, P. Golubkin
Formal analysis: R. P. Raj, P. Golubkin
Funding acquisition: I. E. Kozlov
Investigation: I. L. Bashmachnikov, R. P. Raj, P. Golubkin, I. E. Kozlov
Methodology: I. L. Bashmachnikov, I. E. Kozlov
Project Administration: I. E. Kozlov
Software: I. L. Bashmachnikov
Validation: I. E. Kozlov
Writing – original draft: I. L. Bashmachnikov
Writing – review & editing: I. L. Bashmachnikov, R. P. Raj, P. Golubkin, I. E. Kozlov

1. Introduction

The Nordic Seas are the main gateway through which oceanic heat is channeled into the Arctic, along three branches of the Norwegian Atlantic Current (NwAC) (Gascard & Mork, 2008; Orvik & Niiler, 2002; Raj et al., 2018): the Norwegian Atlantic Slope Current (NwASC), the Norwegian Atlantic Front Current (NwAFC) and a much weaker branch of the Norwegian Atlantic Coastal Current (NwACC) (Figure 1). Of about 8–9 Sv of the overall NwAC transport across the Svinoy section (Dickson et al., 2008; Spall et al., 2021) around 1–3 Sv is directed through the Barents Sea Opening (BSO) into the Barents Sea (Bashmachnikov et al., 2018; Blindheim, 1989; Rudels, 2015; Smedsrud et al., 2013). Around 6–11 Sv is transported north via the West Spitsbergen Current (WSC) (Beszczynska-Möller et al., 2012; Fahrbach, 2006; Rudels, 2015; Schauer et al., 2004, 2008). The large differences in the estimates are due to the different ways of taking into account the strong recirculation in the Fram Strait, as well as different time periods of the averaging. Inter-annual variability reaches 1–2 Sv at Svinoy

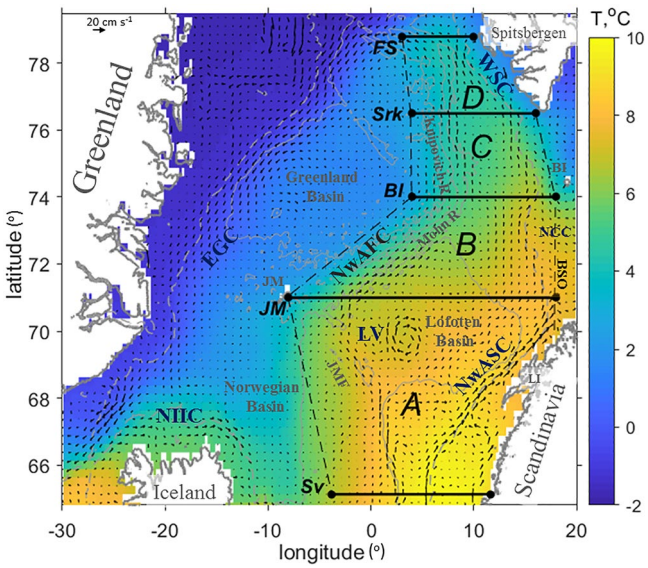

Figure 1. Sea-surface currents (vectors, AVISO altimetry, averaged over 1993–2018) and SST (color, MUR data set, averaged over 2002–2018). NwASC is the Norwegian Atlantic Slope Current, NwAFC is the Norwegian Atlantic Front Current, WSC is the West Spitsbergen Current, EGC is the East Greenland Current, NIIC is the North Icelandic Irminger Current, NCC is the Nordcape Current, LV is the Lofoten Vortex, LI is Lofoten Islands, JMF is the Jan Mayen Fracture zone, BSO is the Barents Sea Opening, Sv is Svinoy section, JM is Jan Mayen section and island, BI is Bear Island section and island, Srk is Sorkapp section, FS is Fram Strait section. A, B, C, D are the areas discussed below. The isobaths of 500 and 2,500 m are marked with gray dashed and solid lines, respectively.

(Skagseth et al., 2008) and up to 5 Sv in the WSC (Beszczynska-Möller et al., 2012; Rudels, 2015). Taking into account this large variability, we suggest an approximate balance of the water transport in and out of the Norwegian Sea. Considering only the Atlantic water (AW) at Svinoy section, defined by the minimum salinity of 34.88 and the minimum temperature of 2°C, from around 8 Sv of the AW, which enters the study region with the NwAC, only 1.5 Sv leaves to the Barents Sea (Rudels, 2015) while 3 Sv enters the Fram Strait with the WSC (Beszczynska-Möller et al., 2012; Kolas & Fer, 2018). The imbalance results from a decrease in the total amount of AW along its path due to cooling and densification associated with direct heat loss to the atmosphere and mixing with surrounding waters (Smedsrud et al., 2022; Spall et al., 2021). The mean AW temperature decreases from 5°C at Svinoy (Mork & Skagseth, 2010) to 3–4°C in the BSO (Bashmachnikov et al., 2018; Skagseth et al., 2008) and 2–4°C in the WSC. This is a result of intense heat loss to the atmosphere (which leads to densification of the AW on its way north), which primarily takes place in the Norwegian Sea (Latarius & Quadfasel, 2016), and, within this region, is concentrated along the branches of the NwAC rather than in the central parts of the basins (Spall et al., 2021).

In terms of the heat fluxes, using the reference temperature Tb = 0°C, the NwAC is estimated to carry around 300 TW across Svinoy section to the Lofoten Basin during the early 1990s and 400 TW in the late 2010s (Bacon et al., 2015; Hansen et al., 2008), while around 140 TW enters the Lofoten Basin from the west (Vesman, 2021). About 20%–25% of this heat (around 124 TW, Tb = 0°C) enters the study region west of the Faroe Islands and forms the NwAFC (Hansen et al., 2015), while the largest heat flux comes in the study region with the NwASC (Spall et al., 2021). The NwACC has significant influence only on the uppermost layer of the Lofoten Basin, while already at 200 m its influence is negligible and the water from the NwASC is clearly dominating (Fedorov et al., 2021). This incoming heat is dispersed around the Norwegian Basin and further is lost to the atmosphere and to mixing with the colder waters of Arctic origin. This results in a decrease of the oceanic heat transport by the WSC through the Fram Strait to around 50 ± 20 TW (Fahrbach, 2006; Rudels, 2015; Schauer & Beszczynska-Möller, 2009; Schauer et al., 2008). Of the overall heat entering the Lofoten Basin from the south, over 75% is lost already within the Lofoten Basin (Vesman, 2021) and only 25% propagates further north across the Bear Island section (Figure 1).

One of the important sources of the heat loss from the NwASC is the oceanic advection into the Barents Sea with the Nordcape Current (NCC), which is 70 ± 20 TW during the recent decades (Tb = 0°C, Bashmachnikov et al., 2018; Smerdsrud et al., 2010). The sum of the oceanic heat loss to the atmosphere and radiation balance over the Norwegian Sea ranges between 50 and 150 W m^{-2}, depending on the season and the position, with the annual and basin-mean heat leaving the ocean surface of around 40–70 W m^{-2} (Latarius & Quadfasel, 2016; Spall et al., 2021; Treguier et al., 2021). This gives an overall heat loss of 30–60 TW at the ocean surface over the eastern Norwegian Sea (regions A and B in Figure 1). A part of the incoming heat is mixed down to supply the core of warm water of the Lofoten Basin below 500 m (Rossby et al., 2009), and also leads to an increase of temperature of the upper layer of the Lofoten Basin, as observed during the recent decades (Mork et al., 2019). The mesoscale eddies generated by baroclinic and barotropic instability of the NwASC and the NwAFC effectively extract the heat from both branches of the NwAC and redistribute it over the Lofoten Basin (Bashmachnikov et al., 2017; Ghaffari et al., 2018; Isachsen, 2015; Kohl, 2007). Both branches of the NwAC, as well as the WSC, meet the instability criteria and can be regarded as eddy generation regions (Ghaffari et al., 2018; Koszalka et al., 2011; Trodahl & Isachsen, 2018). The area of the largest heat loss along the NwAC is also the region of the most intensive generation of eddies by the NwASC, along the steepest section of the continental slope of Norway (Dugstad et al., 2021; Isachsen, 2015; Koszalka et al., 2011; Raj et al., 2020). However, Lagrangian modeling suggests that eddies may be not the only factor in redistributing heat in the basin. Strong pulses of current developed in jets crossing the basin, filaments and Ekman transport may also be of high importance (Dugstad et al., 2021; Fedorov et al., 2021; Spall, 2010).

Chelton et al. (2011) presented one of the first global estimates of statistical characteristics of mesoscale eddies tracked for at least 2 weeks, which means at least two consecutive detections of the same vortex in the 7-day AVISO altimetry. Due to problems with the accuracy of the mean sea-level estimates in the polar regions, this data set has been limited to the coverage area of the TOPEX/Poseidon satellite altimeter, that is, equatorward of 66° latitude, and covers only the southernmost part of the Nordic Seas. Nevertheless, further studies showed that the accuracy of AVISO10 altimetry, tested against in situ sea-level records, is on average 2–3 cm in the Nordic Seas (Volkov & Pujol, 2012), that is, on the same level as in the tropical areas of the ocean (Fu and Cazenave, 2001). The 0.25° × 0.25° spatial resolution of the AVISO data yields 28 km in latitude and, in the Nordic Seas, 10–25 km in longitude. The convergence of satellite tracks in these northern regions increases spatial resolution, which partly compensates for the absence of TOPEX/Poseidon-Jason data series, and the accuracy remains high. This resolution is marginal for the detection of mesoscale eddies with a typically observed dynamic diameter between 20 and 80 km, with 30 km on average (Bondevik, 2011; Johannessen et al., 1983, 1987; Raj & Halo, 2016; Richards & Straneo, 2015; Sandven et al., 1991; Wang et al., 2020; Yu et al., 2017). Recent studies suggest that a further increase in the spatial coverage of the satellite altimetry data set, improvement in the geoid determination (Raj et al., 2018; Taburet et al., 2019) and in the methodologies for automated eddy detection enable AVISO altimetry to obtain correct spatial statistics of mesoscale eddy properties even at these high latitudes, when compared to SAR observations and high-resolution models (Bashmachnikov et al., 2020; Kubryakov et al., 2021). Furthermore, independent observations show that mesoscale eddies detected in the Nordic Seas in sea surface drifter trajectories show a good correspondence with positions of eddies detected in AVISO14 altimetry (Capet et al., 2014; Raj & Halo, 2016).

In the Lofoten Basin, the eddy kinetic energy (EKE) is high, in particular in the north-eastern and northern parts of the basin. Eddies drift from their principal generation region at the Lofoten Islands, circling the basin in a counterclockwise direction. This has been derived from analysis of drifter trajectories (Koszalka et al., 2011; Rossby et al., 2009), altimetry (Raj & Halo, 2016; Raj et al., 2016, 2020) and ocean models (Bashmachnikov et al., 2017; Isachsen, 2015; Kohl, 2007; Raj et al., 2020; Volkov et al., 2015). Eddies are also actively formed further north, in the WSC (Trodahl & Isachsen, 2018). Here eddy transport governs a recirculation branch in the southern part of the Fram Strait (Boyd & D'Asaro, 1994; Nilsen et al., 2006; Hattermann et al., 2016; Kolas & Fer, 2018; Hofmann et al., 2021; von Appen et al., 2015, 2016; Walczowski, 2014).

In this study, we present the statistics of 3D properties of mesoscale eddies in the Lofoten Basin derived from the modern AVISO18 altimetry data and from in situ vertical profiles, and explore eddy heat transport in the Norwegian and Greenland Seas. We show that this flux is significant and its variability may affect the ocean heat transport into the Arctic Ocean.

2. Data and Methods

2.1. The Study Region

Oceanic heat fluxes are estimated across the boundaries of four areas along the AW pathway as it transits through the Nordic Seas from the Svinoy section to the Fram Strait (Figure 1). The western boundary of the study region passes from the western tip of the Svinoy section to Jan Mayen and from Jan Mayen northwards, along Knipovich and Mohn ridges. The eastern boundary follows the Norwegian coast, the Barents Sea Opening, and the western coast of Spitsbergen.

2.2. The Background Characteristics of the Study Region

The vertical extent of temperature-related eddy anomalies roughly corresponds to the thickness of the AW layer in the NwAC, which in the study region extends down to around 500 m (Iakovleva & Bashmachnikov, 2021). The oceanic heat advection over the upper 500 m across the selected sections (Figure 1) was estimated using ARMOR3D data set (http://marine.copernicus.eu/), which combines in situ and satellite observations at standard depth-levels. The data set has the 0.25° × 0.25° spatial resolution and the monthly temporal resolution. The geostrophic current velocity in ARMOR3D was obtained by extrapolating the AVISO altimetry currents downwards using a previously derived 3D data set of gridded vertical profiles of temperature, salinity and the thermal wind relations (Guinehut et al., 2012; Verbrugge et al., 2017). The data are available from 1993 through the web portal of Copernicus Marine Environment Monitoring Service (Verbrugge et al., 2017). The horizontal

heat fluxes were estimated relative to the water freezing reference temperature $T_{ref} = -1.8$°C (Kinney et al., 2014), as well as relative to the more commonly used $T_{ref} = 0$°C (Rudels, 2015; Schauer & Beszczynska-Möller, 2009; Schauer et al., 2008; Skagseth et al., 2008; Smedsrud et al., 2013). With $T_{ref} = -1.8$°C ($T_{ref} = 0$°C), the heat transport of the Atlantic Water across the Svinoy section (Figure 1) is 320 ± 18 TW (255 ± 15 TW), across the Jan Mayen section is 200 ± 17 TW (150 ± 13 TW), across the Sorkapp section is 62 ± 4 TW (43 ± 3 TW), and across the Fram section is 61 ± 3 TW (38 ± 2 TW). In the literature, when referenced to $T_{ref} = 0$°C, the AW heat transport is estimated as 150 TW across the Svinoy section (Skagseth et al., 2008), 30 to 70 TW across the Barents Sea Opening (Bashmachnikov et al., 2018; Skagseth et al., 2008, 2011; Smerdsrud et al., 2010), and around 30 TW across the Fram Strait section (Walczowski, 2014). The relatively small value at the Svinoy section in the literature is due to a smaller length of the transects used, which did not fully cover the oceanic heat transport into the Norwegian Sea.

The ocean-atmosphere heat exchange, as well as the radiation balance (shortwave and longwave), are derived from the ERA–Interim reanalysis (Dee et al., 2011; Fairall et al., 2003) distributed by the European Centre for Medium-range Weather Forecasts (ECMWF, https://apps.ecmwf.int/datasets/data/interim-full-moda/levtype=sfc/).

2.3. Ocean Data for Eddy Heat Flux Estimates

The eddies were detected using AVISO18 sea level height data (SLH) with daily time resolution, available since January 1993 from Copernicus Marine Services (http://marine.copernicus.eu/). The AVISO18 data set has been completely reprocessed in order to exploit the most recent advances in each of the successive processing steps and to provide a product of homogeneous quality (Taburet et al., 2019). The reprocessing includes modifications of a new mean sea-level reference field, a revised inter-calibration procedure, a new ocean tidal component, and new sensor-specific instrumental and atmospheric corrections. The SLH gridded distributions are based on the merged ERS-1, 2, GFO, CryoSat-2, HY-2A, SARAL/AltiKa, Envisat, and Sentinel-3 along-track altimetry. The TOPEX/Poseidon and Jason altimeters coverage reaches up to 66°N, but at these northernmost latitudes the measurements are only used for removal of the long wavelength errors (e.g., orbit error, altimeter biases) in the final AVISO products (Le Traon & Ogor, 1998).

The vertical structure and temperature anomalies in ocean eddies were estimated using the EN4 Hadley Center database (https://www.metoffice.gov.uk/hadobs/en4/). The database collects all available in situ vertical profiles of temperature and salinity, complementing the more widely used World Ocean Database with a number of other in situ datasets. EN4 data set undergoes a strict quality control procedure and a robust removal of the duplicate stations (Good et al., 2013).

2.4. Eddy Detection and Tracking Techniques

Mesoscale eddies were detected using the automatic method suggested by Nencioli et al. (2010). In this method, eddy centers are detected in the velocity field as the centers of circular or elliptic rotating structures of a limited size. The following criteria are applied: the velocity vectors should change the sign along a section across the eddy center and increase in absolute value away from the center, while the velocity directions should cover the full range of angles in order to ensure a closed rotating structure (for details see Nencioli et al., 2010). This algorithm provides more robust detection for weak eddy structures than alternative algorithms based on Okubo-Weiss parameter (Isern-Fontanet et al., 2006), the "winding angle" technique (Chaigneau et al., 2008) or the threshold algorithm for sea-level anomalies (Chelton et al., 2011). Weak eddies should also be considered as their AVISO altimetry amplitude, among other factors, depends on the distance between the eddy center and the closest altimeter track (Bashmachnikov et al., 2013, 2020). Eddy dynamic radii (R) are estimated as the mean distance from the eddy center to the isoline of zero relative vorticity along the radial rays covering the ellipse with the 10° increment (for details see Bashmachnikov et al., 2017). Statistical distributions of eddy properties derived in this study showed a good qualitative agreement for the Lofoten Basin with the results obtained for the same area by Raj et al. (2016, 2020), Raj and Halo (2016), even though the cited authors used a different eddy detection technique, which combines the identification of sea-level anomalies within closed isolines and low values of the Okubo-Weiss parameter. These agreements confirm the robustness of the eddy statistics obtained.

In the Nordic Seas, altimetry data allow identification of isolate vortices with a dynamic radius over 15 km, that is, the eddy-induced sea-level anomaly of order of 60 km (Bashmachnikov et al., 2020; Raj & Halo, 2016). This

experimental estimate is mainly a result of the non-simultaneous character of observations coming from different tracks covering the region, as well as the data errors of an individual sea-level estimate of around 2 cm. At the moment, algorithms for routine automatic detection of vortices of smaller radii from different satellite data are absent. Attempts to study submesoscale processes with along-track altimetry (Chavanne & Klein, 2010) face the problem of anomalies identification from one-dimensional information, while the number of quasi-simultaneous intersections of altimeter tracks is small. Visual expert identification has been used for detection of eddies in SAR images. However, the possibility for eddy detection in SAR data is limited by wind velocity (2–3 to 12–15 m s^{-1}), eddy size (large eddies are more difficult to detect), and eddy type (cyclones are more readily detected than anticyclones, see Zhurbas et al., 2019; Bashmachnikov et al., 2020; Kozlov et al., 2019). Identification of eddies in SST and ocean color data also has several limitations, the most important of which is frequent cloud cover in the region. Aside from satellites, numerical models have been used to study eddy characteristics. However, modern eddy-resolving models need further validation, while the majority of the long-term simulations often do not have sufficient resolution to reproduce mesoscale eddies, except for the largest ones (Stammer, 2005; Wang et al., 2020).

Eddy translation velocities are estimated using a standard algorithm of identification of the nearest eddy with the same direction of rotation (Bashmachnikov et al., 2017; Nencioli et al., 2010). In the present version of this algorithm, at the following time step, we seek all eddies with the same sign of the relative vorticity anomaly situated within the two dynamic radii of the center of a previously detected eddy. If several eddies comply with these criteria, the closest to the reference eddy is selected. If the distances are equal within the AVISO grid step, then the one downstream of the reference eddy is selected. In the overwhelming majority of the cases the algorithm selected the closest eddy. The 7-day time step between the consecutive maps is adopted, instead of the 1-day time step of the AVISO data set, in order to reduce the effect of small misplacements of eddy centers on the translation velocities when the consecutive positions of the eddy centers are still too close to each other. The resulting estimates of eddy translations are binned to 50 × 50 km mesh. The final time-mean eddy translation velocities are estimated at the cells where at least five eddy displacements are identified.

To derive the eddy vertical structure, vertical profiles of temperature and salinity from the EN4 data set were overlaid on the positions of cyclones and anticyclones detected in AVISO altimetry. The results were obtained only for the eddies with at least one profile in the eddy core, that is, within 0.75 eddy dynamic radii from the eddy center (R, see Section 2.4), and at least one profile in the background, that is, between 1 and 2 eddy dynamic radii (Figures 2a and 2c). From the background profiles, those within the neighboring eddies were preliminary excluded. If several profiles were detected in or outside the eddy, they were averaged. Then the temperature, salinity and density anomalies in eddy cores were analyzed. The upper and the lower limits of the eddy cores were estimated (Bashmachnikov et al., 2017) using the following considerations. Formed mainly as a result of dynamic instability of the NwAC or WSC (Trodahl & Isachsen, 2018), the anticyclones with warmer and saltier cores are observed at the cold side of the front, and cyclones with colder and fresher cores—at its warm side. Below the cores of anticyclones, the isotherms (and isopycnals) are curved downwards relative to the surrounding ocean, while under the cores of cyclones they are curved upwards. Therefore, the sign of the anomalies of the thermohaline characteristics below the eddy core coincides with that in the core. In a subsurface eddy, the isotherms and isohalines above the core are pushed upwards. Due to this uplift, at some level above the core of a subsurface anticyclone, the positive anomaly of the core may change to a negative one relative to the background, even though the core is warmer than the background at the lower levels. To sum up the above, the lower limit of the eddy core is marked at the depth level where the water density and temperature anomalies fall to less than 25% of its maximum in the core, though keeping the same sign (Figures 2b, 2c, 2e,and 2f). For subsurface eddies, the upper limit of the eddy core is taken at the closest to the maximum core level where the corresponding thermohaline anomaly changes its sign. Vortices are considered surface-intensified if no upper limit is detected or if it is detected within 100 m from the sea surface (the typical depth of the upper mixed layer in summer).

For all parameters and results presented below, errors of the mean values over a regular grid were estimated as reflective of the combined effect of temporal variability as well as that of data errors. The error of the mean (e) in each cell of a regular grid is estimated as (Emery & Thomson, 2001):

$$e = \frac{t_{0.95,n-1}\sigma}{\sqrt{n}},$$

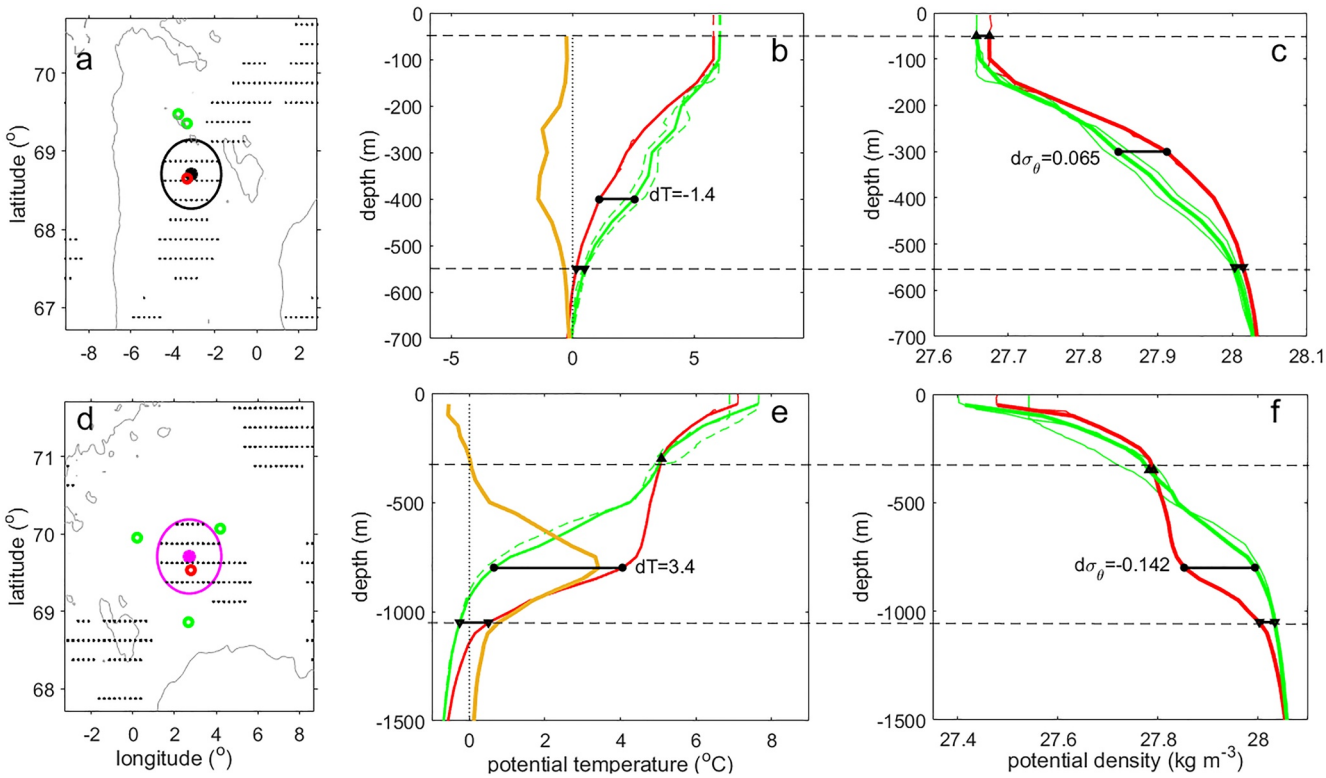

Figure 2. Examples of the detection of the vertical extent of eddy cores: (a–c) for a cyclone detected in AVISO on 18.12.2008 with a peak relative vorticity of 0.17 *f* (where *f* is Coriolis parameter) and (d–f) for an anticyclone detected in AVISO on 30.10.2008 with a peak relative vorticity 0.26 *f*. (a, d) Maps with positions of the eddies (black for the cyclone and magenta for the anticyclone). The areas of the cores of all detected eddies are marked with black dots. The vertical casts inside (red circles) and outside (green circles) eddy cores, used for estimation of the vertical extent, are derived from EN4 data set. Panels (b, e) show vertical profiles of potential temperature (°C) and panels (c, f) show vertical profiles of potential density (kg m^{-3}). Green lines show the background profiles outside the eddies (mean profiles are marked with thick lines) and red lines are for those in the eddy cores. Ochre lines mark the temperature difference between the eddy core and the background. Horizontal dashed lines show the limits of eddy cores (also marked on profiles with triangles) taken for further calculations; horizontal solid lines show the largest temperature (°C) and density (kg m^{-3}) anomalies in eddy cores.

where n is the number of observations in a grid cell, σ is the standard deviation of the variable and $t_{0.95,n}$ is the cumulative Student's distribution for 95% confidence interval and $n-1$ is the number of degrees of freedom. The seasonal cycle of eddy parameters was weak and was not filtered before the error estimates.

3. Eddies in the Nordic Seas From Satellite Altimetry

As a significant amount of the warm AW leaves the branches of the NwAC to fill the interior of the Lofoten basin, a significant drop in the intensity of the heat advection across the Lofoten Basin was detected (Bjork et al., 2001; Kohl, 2007). This drop is accompanied by a rapid meridional drop in correlations between the heat fluxes at the Svinoy and Jan Mayen sections, a result of a significant decrease of the interannual oscillations when crossing the basin (Vesman, 2021). This makes the Lofoten Basin the largest warm water pool in the Norwegian and Greenland Seas, maintained despite the strong annual mean heat release of about 80–90 W m^{-2} (Dukhovskoy et al., 2006; Richards & Straneo, 2015). A significant fraction of the heat extracted from the branches of the NwAC to the interior of the Lofoten Basin is thought to be transported by mesoscale eddies, especially at the Lofoten Islands where eddies are the most intensively generated (Chafik et al., 2015; Isachsen, 2015; Kohl, 2007; Raj et al., 2020). Eddies also play an important role further north, where one of the westward recirculations of the AW in the Fram Strait is considered to be eddy-driven (Boyd & D'Asaro, 1994; Hattermann et al., 2016; Hofmann et al., 2021; Nilsen et al., 2006; von Appen et al., 2015). However, except for some model studies (see, e.g., Hattermann et al., 2016; Spall et al., 2021; Treguier et al., 2021; Wekerle et al., 2020), the effect of coherent eddies on heat redistribution in these areas has not been evaluated and forms the core of this study.

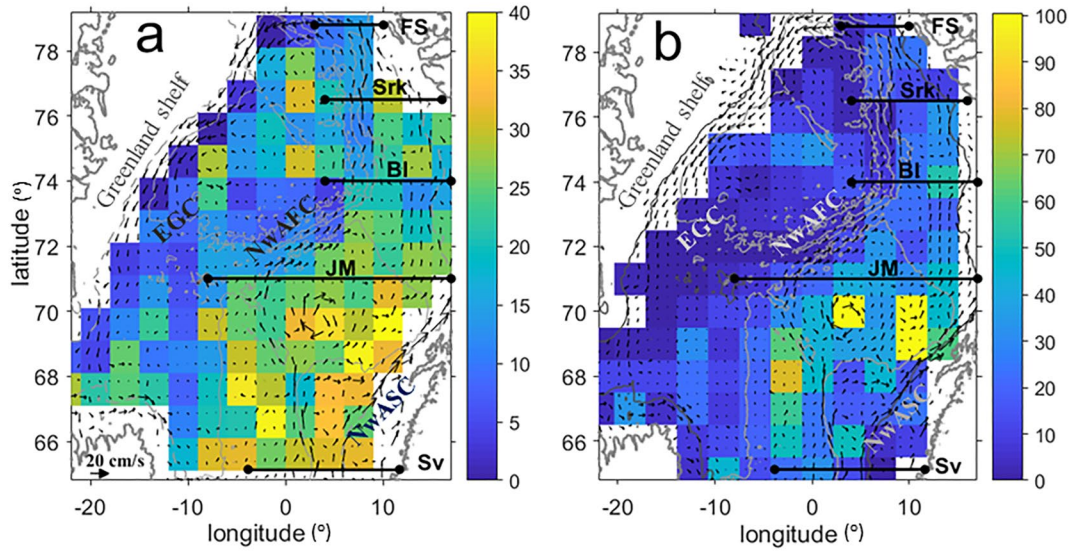

Figure 3. Distribution of mesoscale eddies in the Nordic Seas from satellite altimetry data (1993–2018). (a) Number of eddies per month identified using AVISO altimetry in 1°×3° mesh-boxes. (b) The total number of eddies for which the vertical structure was identified using vertical casts of EN4 data set during the study period. Vectors represent the mean geostrophic currents from AVISO altimetry and black zonal lines are sections for estimating meridional heat fluxes with eddies. For other notations see Figure 1.

Using the AVISO satellite altimetry data, we detected over 900,000 mesoscale eddies in the study region from 1993 to 2018. The total number of the detected eddies in the Norwegian Sea significantly exceeds that in the Greenland Sea (Figure 3a). A decrease in the EKE in the Greenland Sea compared to the Norwegian Sea has been previously noted by Koszalka et al. (2011) from surface drifters. The results of the previous study though remained uncertain due to a low number of drifters in the Greenland Sea. In the eastern part of the study region, the number of eddies with a detected vertical structure exceeds 20 eddies per grid-cell (Figure 3b). This allows estimating the heat transport in this area with a greater confidence compared to large areas of the Greenland Sea where the number of available vertical profiles is lower.

As derived from the altimetry data, the number of anticyclones was, on average, practically equal to that of cyclones throughout the study period. Eddy dynamic radii (R, see Section 2.3) present two peaks at $R = 40$ km and $R = 50$ km (Figure 4a). The first peak reflects eddy radii in the Norwegian Sea (in particular in the Lofoten Basin), and the second one in the Greenland Sea (Figures 4c and 4e). As AVISO altimetry data exaggerates the radii on average by 1.5 times in these northern regions (Bashmachnikov et al., 2020), the real eddy radii distribution should have two peaks around 25–30 km and 30–35 km. On the contrary, the radial extension of the thermohaline anomalies typically exceeds R by 1.4 times which is the e-folding spatial scale of a temperature drop or rise with distance from the eddy center (see Equation 1 below; also see Armi et al., 1989). Given that both issues nearly cancel each other out, we choose to use the computed R as the equivalent radial extent of the thermohaline anomalies in further estimates of the eddy heat transport. None of the eddy radii exceeds the Rhines scale $\sqrt{V_m/2\beta}$~100–200 km, where $V_m = 20$–50 cm s^{-1} is the maximum azimuthal velocity in the eddy core and $\beta = 8\ 10^{-12}$ m^{-1} s^{-1} is the rate of linear change of the Coriolis parameter with latitude, where eddies start demonstrating linear behavior of Rossby waves (Danilov & Gurarie, 2002).

The mean first baroclinic Rossby radius of deformation (Rd) in the study region is around 7–8 km, varying from 7 to 10 km in the south to 5–8 km in the north of the region, depending on water depth and season (Nurser & Bacon, 2014). Thus, the typical expected eddy is about 2.5–3.5 times Rd. Taking into account that the fastest growing dynamic instability of the NwAC in the Lofoten Basin has a wavelength of 15 km, which decreases northwards to 7–10 km west of Spitsbergen (Trodahl & Isachsen, 2018), we may expect the typical radii of the generated eddies to be of the order of Rd, that is, half of this wavelength. The larger detected eddy radii derived in the histograms using satellite data (Figures 4a, 4c, and 4e) can be interpreted as a result of eddy mergers.

Such interpretation is based on eddy merging statistics in other regions of the Atlantic Ocean. For example, the eddy merger leads to an increase in the mean radius of meddies (Mediterranean water eddies in the subtropical North

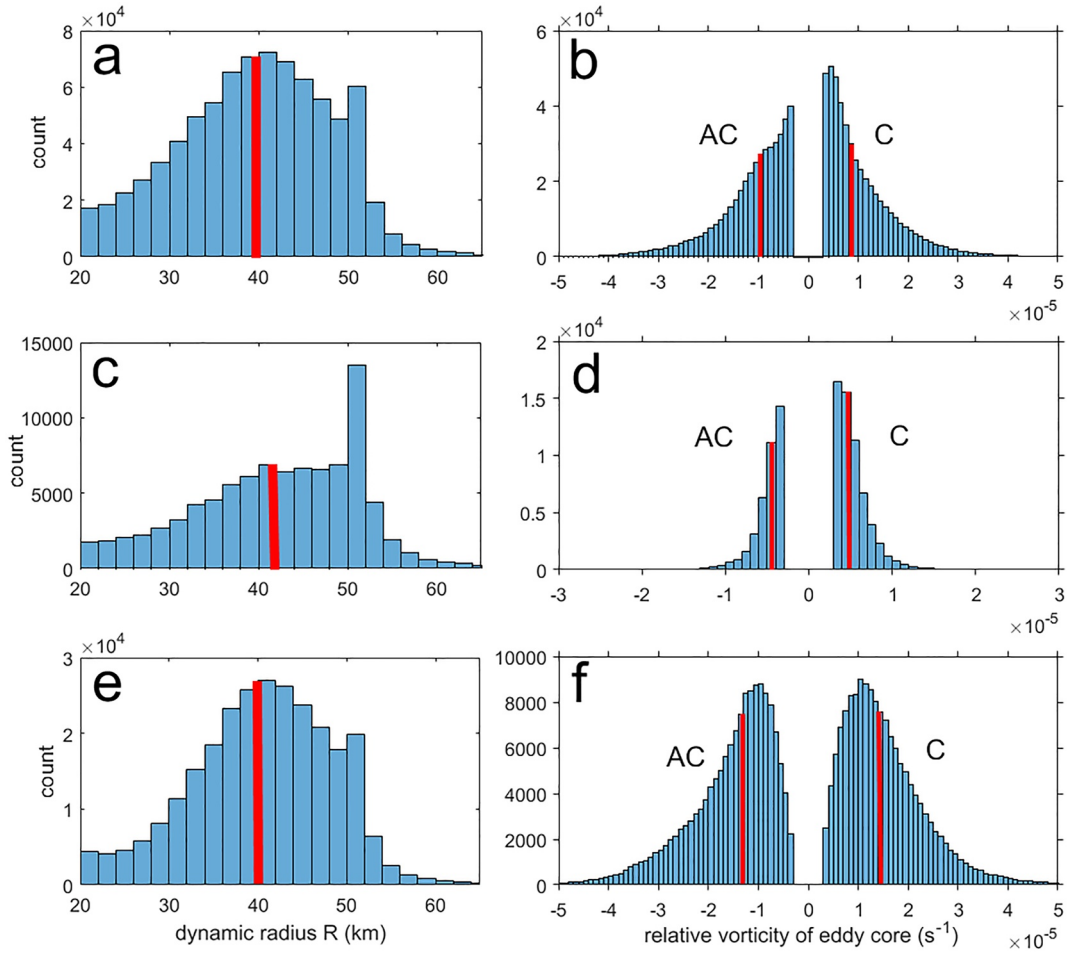

Figure 4. Histograms of (a, c, e) eddy dynamic radii and of (b, d, f) peak relative vorticity of eddies, negative values are anticyclones (AC) and positive are cyclones (C) in the selected areas of the study region (see Figure 1): upper row (a, b) is the whole region of the Nordic Seas; central row (c, d) is the Greenland Basin of the Greenland Sea; lower row (e, f) is the southeastern Norwegian Sea (region A in Figure 1). Red vertical lines show the median values.

Atlantic) at a rate of 10–15 km per each 100 km with the distance from their generation region (Bashmachnikov et al., 2015). At 400–600 km distance from the generation region, the mean meddy radius reaches its maximum of three regional *Rd* (Figure 6a). An increase in eddy radii northwestwards from the NwASC at around 300–400 km distance from the Lofoten Islands (Figures 5 and 6a) is within the distance over which frequent meddy mergers were observed in the subtropical North Atlantic. This is seen in Figure 5, where the second peak of 50 km in areas of known intensive eddy generation (A and D, see Figure 1) is much smaller than in areas where a large part of eddies may be of non-local origin (B and C). It is natural that eddies which increase their size due to eddy mergers have longer lifetimes and thus become more frequent away from the generation region (compare eddy radii at the Scandinavian continental margin and in the western and northwestern part of the Norwegian Sea in Figure 6a). In fact, merges of individual eddies have been often observed in the Lofoten Basin (Bashmachnikov et al., 2017; Kohl, 2007; Raj et al., 2016; Volkov et al., 2015).

The ratio of the peak relative vorticity to the Coriolis parameter (the Rossby number, *Ro*) typically does not exceed 0.15 in the study region. This means that the peak relative vorticity of the majority of the selected vortices is rather weak (Figures 4b and 6b). The exception is the Lofoten vortex with *Ro* over 0.6. Direct in situ observations (Yu et al., 2017) show *Ro* of the Lofoten Vortex reaching 0.7–0.8. In the analyzed altimetry data, the intensity of mesoscale anticyclones in the study region is somewhat greater than that of cyclones. The highest intensity of the absolute values of the relative vorticity of mesoscale eddies is observed along the two branches of the NwAC, and in particular the northern Lofoten Basin (Figure 6b), the region of the most intensive eddy generation

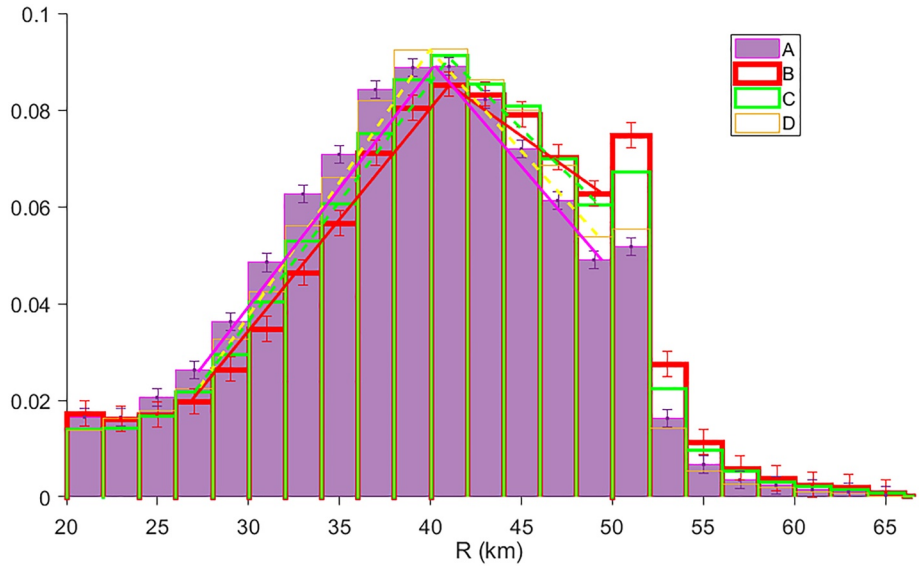

Figure 5. Normalized histogram of eddy dynamic radii in areas A (filled bars), B (empty red bars), C (empty green bars) and D (empty yellow bars). Straight lines connect the top of the bars between the main mode in the histogram and the basement of this peak, highlighting the differences in the shape of the main peak of the areas A and D relative to the areas B and C. Error bars are shown for regions A and B. Regions A–D are shown in Figure 1.

in the Nordic Seas (Trodahl & Isachsen, 2018). Further north the number and intensity of eddies decrease, consistent with the northward decrease of EKE derived from drifter observations (Koszalka et al., 2011), as well as the decreased intensity of the potential energy conversion into the EKE (the baroclinic instability) and the decreased intensity of the kinetic energy conversion into the EKE (the barotropic instability), as derived from high-resolution model studies (Trodahl & Isachsen, 2018). A further slight increase of the eddy relative vorticity in the Fram Strait suggests another area of the intensive eddy generation (previously noted in von Appen et al., 2016).

In the central Greenland Sea, the peak relative vorticity of eddy cores, on average, is about one-half of that in the Norwegian Sea (Figures 4d and 4f, and 6b). Here the number of cyclones, accounting for more than 60% of all

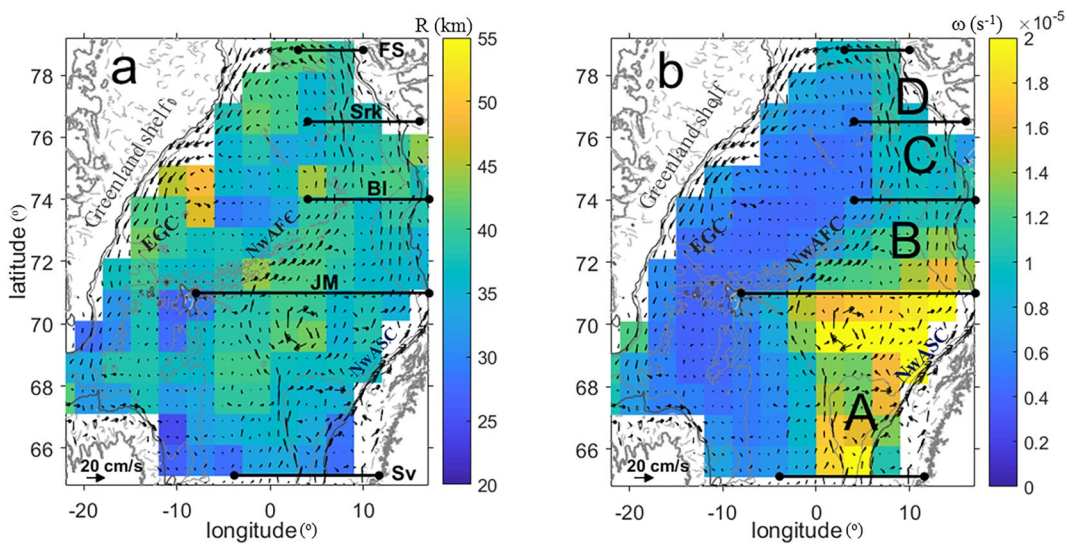

Figure 6. Spatial distribution of (a) eddy dynamic radii (km) and (b) absolute values of eddy peak relative vorticity (s^{-1}). Black vectors show the time mean (1993–2018) current velocity; gray lines show 500 and 2,500 m isobaths. For other notations see Figure 1.

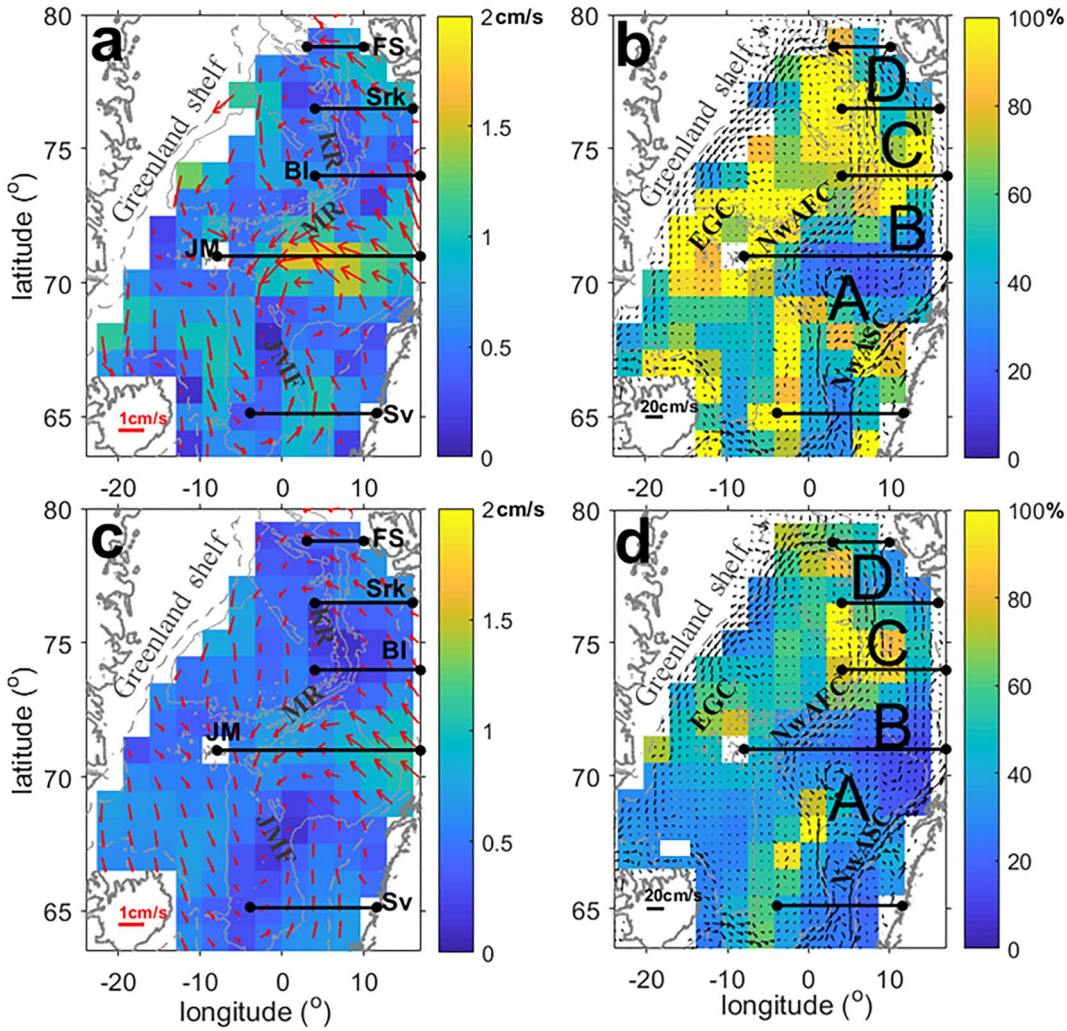

Figure 7. Velocities (cm s^{-1}) and directions of eddy translation averaged over 1993–2018. (a, c) Mean vectors of the eddy translations (red arrows, color is current velocity, cm s^{-1}) and (b, d) relative errors of the mean in % of the mean values at 50 × 50 km mesh with different smoothing windows: (a, b) 220 × 220 km and (c, d) 440 × 440 km. Only the cells with five or more registered eddy displacements in the average are considered in the plot. Black arrows in panels (b and d) are the background mean currents derived from AVISO altimetry. Gray lines show 500 and 2,500 m isobaths. MR is the Mohn Ridge, KR is the Knipovich Ridge. For other notations see Figure 1.

detected eddies, clearly exceeds that of anticyclones (Figure 4d), while in the Norwegian Sea this ratio is close to unity (Figure 4f). The latter was also previously noted in Dugstad et al. (2021).

Eddy translation velocities (Figures 7a and 7c) are found to be directed away from the eastern boundary. Two particular dense and regular eddy translation paths are directed west from the Lofoten Islands and the western Spitsbergen, both known as areas of the intensive eddy generation (Boyd & D'Asaro, 1994; Hattermann et al., 2016; Isachsen, 2015; Trodahl & Isachsen, 2018; Nilsen et al., 2006; von Appen et al., 2015). There, eddy translation velocities are higher than over most of the region. Eddies enter the Norwegian and Greenland Seas from the south with the NwAC, from the east through the Barents Sea Opening, and from the north with the EGC (Bondevik, 2011; Johannessen et al., 1983, 1987; Kozlov & Atadzhanova, 2022; Sandven et al., 1991; von Appen et al., 2018).

Eddies tend to follow the main topographic features and the topographically trapped currents in a counterclockwise direction around the Nordic Seas. A pronounced counterclockwise eddy circulation is observed in the Lofoten Basin, consistent with previous studies (Kohl, 2007; Raj & Halo, 2016), as well as in the northern Greenland Sea. Observations and theoretical estimates suggest that self-translation velocities of mesoscale eddies, that is,

velocities of a directional propagation of eddy cores due to internal mechanisms (Cushman-Roisin et al., 1990), can be high enough to allow eddies to move against the mean flow (Bashmachnikov et al., 2015; Morel & McWilliams, 1997). The predominant movement of the mesoscale eddies with the mean currents in the subpolar study region is linked to an increase in the importance of the topographic β-effect in eddy self-translations with latitude compared to the planetary one. The planetary β-effect often governs the self-translations of mesoscale eddies in the subtropics (Bashmachnikov et al., 2015; Morel & McWilliams, 1997), while in the Nordic Seas the topographic β-effect makes eddies skirt the Norwegian-Greenland basin in a cyclonic direction, along with the mean current. The characteristic eddy translation velocities of 1–3 cm s^{-1} (Figures 7a and 7c) are in the range of the typical eddy translation velocities (Bashmachnikov et al., 2014; Chelton et al., 2011; Raj et al., 2020) and are much smaller than the velocity of the NwAC of 5–20 cm s^{-1} (Figure 7b). The westward deviation of the eddy translation velocities from the NwASC between 67°N and 75°N agrees with the results of Isachsen et al. (2012), which were based on drifter trajectories, altimetry and a high-resolution numerical model. This eddy translation is steered by the deep topography of the northern Lofoten Basin, as well as across the Fram Strait (Figures 7a and 7b). Although the mean velocities obtained from the two smoothing windows (220 × 220 km^2 and 440 × 440 km^2) are qualitatively similar (Figures 7a and 7c), the errors of the mean are significantly higher when the smaller smoothing window is used. In the former case, errors reach 100% of the signal along the eastern boundary of the region, while for the larger window the error is around 10%–50% (Figures 7b and 7d).

4. Eddy Heat Fluxes

Ocean vortices may be an important agent of heat transport (Dutkiewicz et al., 2001; Spall & Chapman, 1998). In this section, we explore the possible role of mesoscale eddies in heat redistribution in the Norwegian and Greenland Seas. Vertical extent and thermohaline properties of eddy cores were obtained only for about 4% of the detected eddies which, nevertheless, form several thousand cases. The eastern Norwegian Sea, which is more densely populated with eddies than other parts of the region (Figure 3a), is also more densely sampled. Here the number of eddies with vertical profiles is several times that of the Greenland or Iceland Seas (Figure 3b). Nevertheless, even 10 to 30 observations per grid cell in the Greenland Sea permit derivation of a consistent large-scale spatial pattern of the time-mean 3D characteristics of eddies over the study region.

The majority of eddies (over 75%) are classified as surface or near-surface intensified ones. The typical vertical thickness of the eddies in the central Greenland Sea and the Iceland Sea is 100–400 m, smaller than those in the eastern part of the region, including the Lofoten basin, where it is around 500 m (Figure 8a). The error is, on average, 127 m and forms around 30% of the mean (Figure 8b) and the signal to noise ratio is robust over most of the region. The exception is the central Greenland Sea, where errors are comparable to the mean vertical extent of eddy cores. The maximum eddy thickness of about 800 m is reached in the western Lofoten Basin. In the Norwegian Sea, eddy cores typically have relatively high temperature and salinity (Figure 8c), forming predominantly positive anomalies. In the Greenland Sea, the mean temperatures in the eddy cores are typically close to the background, while negative temperature anomalies of eddy cores relative to the background are often observed. The error of the mean for the temperature of eddy cores is low over most of the study region (Figure 8d). In the Greenland Sea, despite the high relative signal-to-noise ratio, the consistently low temperature values in the eddy cores suggest they are realistic (Figures 8c and 8d).

The azimuthal velocity of quasi-geostrophic mesoscale eddies typically has the Rayleigh radial profile (Bashmachnikov & Carton, 2012; Carton et al., 1989; Paillet et al., 2002), which assumes the Gaussian azimuthal distribution of scalar parameters, such as temperature (Shapiro & Meschanov, 1996):

$$T(r,z) = T_0(z)e^{-r^2/2R^2}, \tag{1}$$

where $T_0(z)$ is the temperature in the central part of the eddy core with the dynamic radius R at depth level z, r is the radial distance from the eddy center.

Then the integral of temperature over the section across the eddy center is:

$$T_{\text{int}}(z) = 2\int_0^R (T(r,z) - T_{\text{ref}})dr = R\left(\sqrt{2\pi}\,\text{erf}(1/\sqrt{2})T_0(z) - 2T_{\text{ref}}\right) \approx 1.7R(T_0(z) - 1.17T_{\text{ref}}) \tag{2}$$

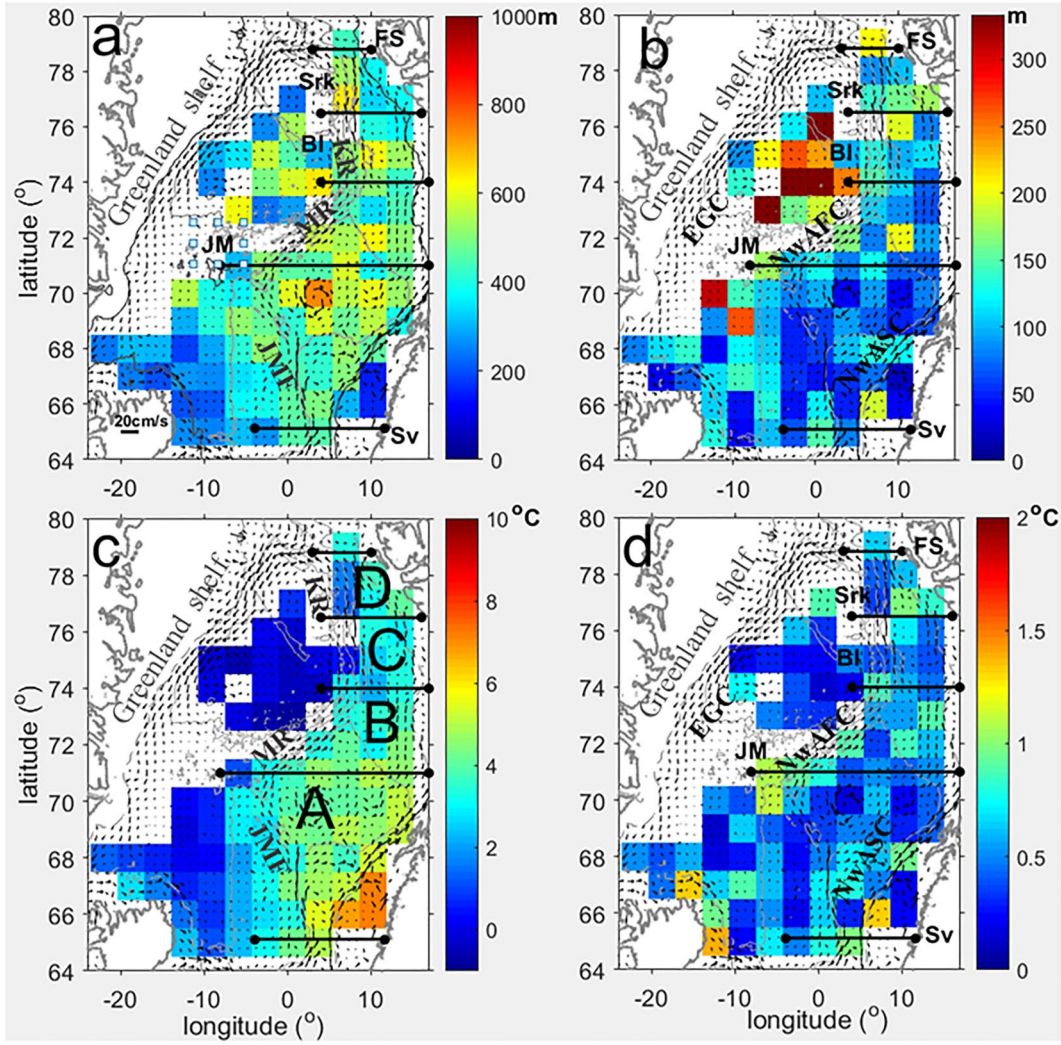

Figure 8. Spatial distribution of eddy 3D properties: (a) mean values and (b) errors of the mean for the vertical thickness of eddy cores (m); (c) mean values and (d) errors of the mean for the depth averaged temperature in eddy cores (°C). The cells with fewer than five eddies for which the vertical characteristics could be derived are blanked. Black vectors show the time mean (1993–2018) AVISO current velocity; gray lines show 500 and 2,500 m isobaths. For other notations see Figure 1.

Following Abernathey and Haller (2018), the eddy heat flux is computed as the maximum amount of heat per time passing across a vertical section with propagating eddies:

$$Q = n\,V_e \int_{Z_{\text{low}}}^{Z_{\text{up}}} C_p\,\rho T_{\text{int}}(z)dz \approx 1.7n\,V_e\,R \int_{Z_{\text{low}}}^{Z_{\text{up}}} C_p\,\rho(T_0(z) - T_{\text{ref}})dz, \quad (3)$$

where $C_p = 4200$ J °C^{-1} kg^{-1} is the specific heat capacity of ocean water, $\rho = 1{,}030$ kg m^{-3} is the mean water density, $T_{\text{ref}} = -1.8$°C is the reference temperature, V_e is the eddy self-translation velocity, n is the number of eddy centers detected in a grid cell per week. The heat content is integrated in the vertical from the lower (Z_{low}) to the upper (Z_{up}) limits of eddy cores. All the parameters are preliminarily averaged in each grid cell, after which the eddy heat transport is estimated. This decreases a random noise linked to possible errors in the determination of the parameters of Equation 3. The results are shown only when at least five individual estimates in a grid cell are available.

The integral eddy heat transport from the shelf-break-trapped NwASC (from Svinoy to Fram Strait sections) is estimated to be around 70 ± 23 TW and has the general direction to the west or north-west (Table 1). 80%–90% of

Table 1
The Total Eddy Heat Fluxes (TW) From the NwAFC (Q_F), From the NwASC (Q_S), and the Northward Eddy Heat Flux (Q_N), Across the Zonal Sections (FS, Srk, BI, JM and Sv)

Region	Q_F, TW	Q_S, TW	Q_N, TW	dQ, TW	Q_{atm}, TW	dQ/Q_{atm}, %
Fram Strait section (FS)			–			
Region D	–	–		–	18 ± 3	–
Serkapp section (Srk)			2* ± 2			
Region C	2* ± 3	7 ± 4		5* ± 4	12 ± 2	42* ± 19%
Bear Island section (BI)			2* ± 4			–
Region B	1* ± 1	11 ± 4		10 ± 4	21 ± 2	48 ± 15%
Jan Mayen section (JM)			2* ± 3			
Region A	14 ± 7	49 ± 15		42 ± 10	41 ± 5	102 ± 24%
Svinoy section (Sv)			9* ± 10			

Note. The convergence of eddy heat fluxes in areas A-D (Figure 9a), marked as dQ, and their ratio to ocean heat release to the atmosphere (Q_{atm}) are also shown. Q_{atm} represents the sum of latent and sensible heat fluxes with the radiation balance integrated over regions A-D (positive is from the ocean). The eddy fluxes in region D could not be estimated due to a low number of eddies with derived vertical structure in this area. Uncertain fluxes are marked with "*."

this flux is produced along the continental slope of the Scandinavian Peninsula, mainly in the northern Lofoten Basin (Figure 9a). This flux is comparable to the overall heat flux entering the Barents Sea when using the same reference temperature of −1.8°C (Bashmachnikov et al., 2018; Smerdsrud et al., 2010), and constitutes around 20% of the total heat (320 ± –18 TW with T_{ref} = -1.8°C) passing through Svinoy section and 35% of the heat flux passing through Jan Mayen section. Considering only the NwASC, the average total advective heat transport of the NwASC is found to be around 175 TW across the Svinoy section, 125 TW across the Jan Mayen section, and around 50 TW across the Sorkapp section. Therefore, the mesoscale eddy transport accounts for around 40 ± 15%, 55 ± 20% and over 100% of the total advective heat transport across the sections above, respectively. The difference between the advection of the NwASC through the Svinoy and Jan Mayen sections is 50 TW (region A in Figure 9). According to our estimates, this is about the same as the amount of heat that leaves the NwASC with eddies. Further north, between the Jan Mayen and Sorkapp sections, about 70–100 TW of heat enters the Barents Sea (Bashmachnikov et al., 2018; Skagseth, 2008). This is of the same order of magnitude as the heat loss from the NwASC to the central Lofoten Basin, extracted out by mesoscale eddies (Table 1). However, Figures 7 and 9a show eddy heat flux entering area B from the Barents Sea. Eddies cross the NwASC and propagate further west in a cyclonic loop. Therefore, some of the heat advected into the Barents Sea with the Nordcape current is returned back into the Norwegian Sea. The westward eddy heat flux from the NwAFC into the Iceland and Greenland Seas is only about 25% of that from the NwASC (between the Svinoy and Sorkapp sections). At least part of this heat is extracted from the NwAFC by eddies, which are generated locally. Some fraction of the flux may also be linked to the eddies from the NwASC which cross the ridge bordering the western Lofoten Basin. Overall low values of the eddy heat flux from the NwAFC suggest that most of the heat from the NwASC is dispersed by eddies between the NwAFC and NwASC, primarily in the Lofoten Basin.

When compared to the heat loss to the atmosphere (Table 1), the eddy heat flux from the NwASC in regions A and B is on the same order of magnitude as the overall ocean heat loss to the atmosphere from these two regions.

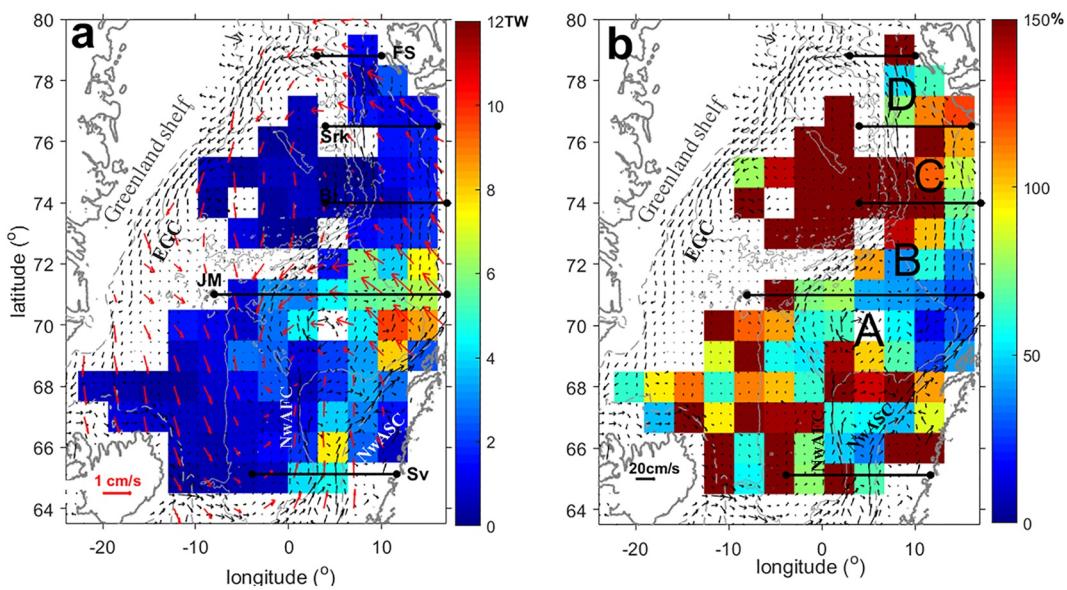

Figure 9. Eddy heat transport Q (TW) derived from Equation 3. (a) Spatial distribution of the eddy heat transport with vectors of eddy velocities overlaid (500 × 500 km sliding means). Black vectors show the time mean (1993–2018) current velocity; gray lines show 500, 1,000 and 2,000 m isobaths. (b) Relative error of the mean in % of the mean values.

Previously, such balance was suggested by Richards and Straneo (2015), who combined data from one mooring in Lofoten Basin with climatological atmospheric fluxes. To complete the balance, we should add to the eddy heat flux around 5 TW which is lost by the NwASC directly to the atmosphere. The NwAFC apparently does not add much to the heat balance of the Lofoten Basin. Previous studies of the Lagrangian tracked particles (Fedorov et al., 2021) suggest that only a small fraction of particles enters the Lofoten Basin from the NwAFC. In region B, the eddy heat flux from the south along the eastern part of the section (not shown) is of the same order as the westward one by eddies locally generated along the NwASC (Figures 7 and 9a). However, most of this heat is transported back into the central Lofoten Basin further west, giving a relatively modest heat surplus of the order of a few TW (Table 1). In regions C and D, the eddy heat transport from the NwASC is uncertain due to a low number of observations (Figure 3b). In region D eddies are known to be effectively generated at the West Spitsbergen Current and further drift westwards (Bashmachnikov et al., 2020; Hattermann et al., 2016; von Appen et al., 2015, see also Figures 7a and 7c).

Having estimated the time mean fluxes above, we do not have sufficient data for estimating their interannual variability. Altimetry data suggest that in regions A-D the annual mean number of simultaneously observed eddies does not change much from year to year and is typically within 15%. If other parameters (eddy radii, thickness, translation velocity, core temperature) remain relatively constant, the interannual variability accounts for about 10 TW. This should not significantly change the heat extracted out of the NwAC by eddies. The annual mean eddy radius practically does not change over the period of observations, and we can further assume that the vertical extent and eddy translation velocities also remain somewhat constant with time. We may also expect proportional changes of temperature in the eddy cores to those in the NwASC. Increasing temperature in eddy cores by 1°C along the path of the NwASC leads to an increase of eddy heat transport by 50 TW. This flux can be further intensified as an increase in the temperature of the AW increases the instability of the NwASC (Isachsen, 2015). This estimate above is comparable with the 40 TW of the interannual variability in the heat advection of the NwASC (Skagseth et al., 2008). Therefore, eddies may effectively damp temperature variations of the advected waters. A northward damping of temperature anomalies along the NwAC was previously derived from an analysis of the interannual variability of the northward heat advection in the Norwegian Sea (Vesman, 2021).

5. Summary and Conclusions

In this study, we evaluate the mean characteristics and transport properties of eddies in the Norwegian and Greenland Seas during 1993–2018, as well as their possible effect on heat transport of the two branches of the NwAC into the Arctic.

Our statistics of 2D eddy characteristics in the Norwegian and Greenland Seas is the most complete to date. In the Norwegian Sea, the eddy characteristics and translation patterns closely correspond to the results obtained from surface drifters by Koszalka et al. (2011). Our results extend on previous altimetry-based analyses of Raj et al. (2020) in the Lofoten basin and of Bashmachnikov et al. (2020) in the northern Greenland Sea and Fram Strait.

Our study shows that the mesoscale eddies in the Greenland Sea are much less numerous and less intense compared to the Norwegian Sea. The smaller number of eddies in the Greenland Sea is consistent with our knowledge that the most efficient eddy generation is concentrated in the eastern part of the basin, and is linked to instability of the NwASC and WSC. This has been derived from observations, high-resolution numerical ocean models and theoretical analysis (Isachsen, 2015; Ghaffari et al., 2018; Hattermann et al., 2016; Trodahl & Isachsen, 2018; Koszalka et al., 2011; von Appen et al., 2015). A limited exchange between the Greenland Sea and the Norwegian Sea could be deduced from our analysis of eddy properties (Figure 7) and is conditioned by a relatively weak westward eddy heat flux from the NwAFC compared to the NwASC (Figure 9a and Table 1).

In the Lofoten Basin, eddy radii grow along the westward and northwestward eddy propagation paths. This indicates that eddies generated in the NwASC undergo mergers before reaching the western side of the basin. This suggests that besides the observed multiple mergers of the quasi-permanent Lofoten Vortex with other anticyclones (Bashmachnikov et al., 2017; Kohl, 2007; Raj et al., 2015; Trodahl et al., 2020; Volkov et al., 2015), mergers of other eddies as they travel from their generation sites is a persistent feature. A similar process has been observed for meddies in the subtropical Atlantic (Bashmachnikov et al., 2015).

This study also gives the first analysis of 3D statistics of the eddies over the entire Norwegian and Greenland Seas based on in situ data. Statistics for the northernmost and westernmost areas of the Greenland Sea cannot be

obtained because of a low number of observations of vertical structure of eddies in these areas. A decrease in the vertical extent of eddies in the Greenland Sea, compared to that in the Norwegian Sea, does not have a straightforward explanation. A weaker stratification of currents in the Greenland Sea should favor thicker eddy cores generated locally. The very low or negative temperature of eddy cores and predominantly southward direction of propagation in the Greenland Sea suggest the local origin of the eddies rather than their generation from the NwAFC. Heat balance estimates (Section 4) also suggest that the Norwegian-Greenland heat exchange across the Polar front is small although the errors of the presented estimates are large.

The NwASC, in contrast, loses a significant fraction of heat with eddy transport into the Norwegian Sea. From the Svinoy to Sorkapp section about 70 ± 23 TW are extracted from the Norwegian current by mesoscale eddies and transported west or northwest which accounts for 35% of the heat advected by the NwASC across the Svinoy section and 100% of that across the Sorkapp section. This is also comparable with 70–100 TW of the heat (for the same reference temperature of -1.8°C) extracted into the Nordcape Current through the Barents Sea Opening (Bashmachnikov et al., 2018; Smerdsrud et al., 2010). The derived eddy heat transport from the NwASC forms about the half of the overall annual mean sea-surface heat loss to the atmosphere over the Greenland and Norwegian Seas (Smedsrud et al., 2022).

Eddy heat flux from the NwASC cannot fully close the heat balance of the Lofoten Basin (Dugstad et al., 2021; Spall, 2010). The required amount, according to Vesman (2021), should be three times the heat flux estimated here. Eddies generated to the south of the basin and in the NwAFC, as well as other transient dynamic patterns (jets, filaments, submesoscale diffusion), should be added, but they also cannot fully close the regional heat budget (Dugstad et al., 2021; Spall, 2010). Analysis of SAR images and the results of high-resolution FESOM numerical model suggest that eddies with radii of 2–5 km are the most frequent in this region (Bashmachnikov et al., 2020). A single small eddy is a short-living structure (up to 5–7 days, Eldevik & Dysthe, 2002). During its lifetime such eddy propagates only a few kilometers and, accounting for its relatively small size, we may expect two to three orders of magnitude less efficient heat transport compared to a single mesoscale eddy analyzed here. However, model studies suggest that, due to a large number of submesoscale structures, their integral effect on the heat transport could exceed that of mesoscale eddies (Dugstad et al., 2021; Spall, 2010).

The analysis suggests a rather large dispersion of eddy properties in each point of the mesh (Figures 7b, 7d, 8b, and 8d), as well as large associated errors in determining eddy characteristics. This leads to significant errors in the estimated time-average heat fluxes (Figure 9b and Table 1). The collocated number of the vertical profiles has been improved during the recent decade due to a more regular sampling of the region with Argo floats. Further improvement could be achieved when the data from the high-resolution SWOT altimetry mission will become available (Ma et al., 2020; Morrow et al., 2019).

Our results on the 3D structure of mesoscale eddies are not sufficient to estimate interannual variability of the properties of eddy cores or the related heat fluxes. Nevertheless, the conducted sensitivity analysis has demonstrated that the relatively small interannual variability in the number of the generated eddies could account only for about 10 TW of the year-to-year difference in the eddy heat transport from the NwASC. Therefore, we assume that the change in the NwASC transport only weakly affects the eddy generation intensity and the related heat flux. However, rough estimates by using climatological mean eddy radii, vertical extent and translation velocities, suggest that the heat release with eddies may potentially damp temperature anomalies that propagate north along the NwASC (Vesman, 2021).

Data Availability Statement

Archiving, Validation and Interpretation of Satellite Oceanographic data (AVISO) database, used for eddy detection, and ARMOR3D, used for computation of advective heat fluxes, are freely available from Copernicus Marine Services (https://data.marine.copernicus.eu/product/MULTIOBS_GLO_PHY_TSUV_3D_MYNRT_015_012/services). The vertical structure and temperature anomalies in eddies were estimated using the EN4 Hadley Center database, available at https://www.metoffice.gov.uk/hadobs/en4/. Sea-surface currents are derived from AVISO altimetry data set (https://www.aviso.altimetry.fr/en/data/products), while sea surface temperature is downloaded from Multi-scale Ultra-high Resolution (MUR) data set (https://podaac.jpl.nasa.gov/MEaSUREs-MUR). ERA–Interim reanalysis used in this study is distributed by the European Centre for Medium-range Weather Forecasts (ECMWF, https://apps.ecmwf.int/datasets/data/interim-full-moda/levtype=sfc/).

Acknowledgments
This study was supported by the Russian Science Foundation (RSF) project # 21-17-00278, https://rscf.ru/project/21-17-00278/. The authors also acknowledge three anonymous reviewers that helped to improve this manuscript.

References

Abernathey, R., & Haller, G. (2018). Transport by Lagrangian vortices in the eastern Pacific. *Journal of Physical Oceanography*, *48*(3), 667–685. https://doi.org/10.1175/jpo-d-17-0102.1

Armi, L., Hebert, D., Oakey, N., Price, J. F., Richardson, P. L., Rossby, H. T., & Ruddick, B. (1989). Two years in the life of a Mediterranean salt lens. *Journal of Physical Oceanography*, *19*(3), 354–370. https://doi.org/10.1175/1520-0485(1989)019<0354:tyitlo>2.0.co;2

Bacon, S., Aksenov, Y., Fawcett, S., & Madec, G. (2015). Arctic mass, freshwater and heat fluxes: Methods and modelled seasonal variability. *Philosophical Transactions of the Royal Society A: Mathematical, Physical & Engineering Sciences*, *373*(2052), 20140169. https://doi.org/10.1098/rsta.2014.0169

Bashmachnikov, I., Boutov, D., & Dias, J. (2013). Manifestation of two meddies in altimetry and sea-surface temperature. *Ocean Science*, *9*(2), 249–259. https://doi.org/10.5194/os-9-249-2013

Bashmachnikov, I., & Carton, X. (2012). Surface signature of Mediterranean water eddies in the Northeastern Atlantic: Effect of the upper ocean stratification. *Ocean Science*, *8*(6), 931–943. https://doi.org/10.5194/os-8-931-2012

Bashmachnikov, I., Carton, X., & Belonenko, T. (2014). Characteristics of surface signatures of Mediterranean water eddies. *Journal of Geophysical Research: Ocean*, *C119*(10), 22–7266. https://doi.org/10.1002/2014JC010244

Bashmachnikov, I., Neves, F., Calheiros, T., & Carton, X. (2015). Properties and pathways of Mediterranean water eddies in the Atlantic. *Progress in Oceanography*, *137*, 149–172. https://doi.org/10.1016/j.pocean.2015.06.001

Bashmachnikov, I., Sokolovskiy, M. A., Belonenko, T. V., Volkov, D. L., Isachsen, P. E., & Carton, X. (2017). On the vertical structure and stability of the Lofoten vortex in the Norwegian Sea. *Deep-Sea Research I*, *128*, 1–27. https://doi.org/10.1016/j.dsr.2017.08.001

Bashmachnikov, I. L., Kozlov, I. E., Petrenko, L. A., Glok, N. I., & Wekerle, C. (2020). Eddies in the North Greenland Sea and Fram Strait from satellite altimetry, SAR and high-resolution model data. *Journal of Geophysical Research: Oceans*, *125*(7), e2019JC015832. https://doi.org/10.1029/2019jc015832

Bashmachnikov, I. L., Yurova, A. Y., Bobylev, L. P., & Vesman, A. V. (2018). Seasonal and interannual variations of heat fluxes in the Barents Sea Region. *Izvestiya - Atmospheric and Oceanic Physics*, *54*(2), 213–222. https://doi.org/10.1134/s0001433818020032

Beszczynska-Möller, A., Fahrbach, E., Schauer, U., & Hansen, E. (2012). Variability in Atlantic water temperature and transport at the entrance to the Arctic Ocean, 1997–2010. *ICES Journal of Marine Science*, *69*(5), 852–863. https://doi.org/10.1093/icesjms/fss056

Bjork, G., Gustafsson, B. G., & Stigebrandt, A. (2001). Upper layer circulation of the Nordic Seas as inferred from the spatial distribution of heat and freshwater content and potential energy. *Polar Research*, *20*(2), 161–168. https://doi.org/10.3402/polar.v20i2.6513

Blindheim, J. (1989). Cascading of Barents Sea bottom water into the Norwegian Sea. *Rapports et Proces-Verbaux des Reunions Consell International pour l'Exploration de la Mer*, *188*, 49–58.

Bondevik, E. (2011). Studies of eddies in the marginal ice zone along the east Greenland current using spaceborne synthetic aperture radar (SAR). (Master's thesis). The University of Bergen.

Boyd, T., & D'Asaro, E. A. (1994). Cooling of the west Spitsbergen current: Wintertime observations west of Svalbard. *Journal of Geophysical Research*, *99*(C11), 22597–22618. https://doi.org/10.1029/94jc01824

Capet, A., Mason, E., Rossi, V., Troupin, C., Faugère, Y., Pujol, I., & Pascual, A. (2014). Implications of refined altimetry on estimates of mesoscale activity and eddy-driven offshore transport in the eastern boundary upwelling systems. *Geophysical Research Letters*, *41*(21), 7602–7610. https://doi.org/10.1002/2014GL061770

Carton, X. J., Flierl, G. R., & Polvani, L. M. (1989). The generation of tripoles from unstable axisymmetric isolated vortex structures. *EPL*, *9*(4), 339–344. https://doi.org/10.1209/0295-5075/9/4/007

Chafik, L., Nilsson, J., Skagseth, Ø., & Lundberg, P. (2015). On the flow of Atlantic water and temperature anomalies in the Nordic seas toward the Arctic Ocean. *Journal of Geophysical Research: Oceans*, *120*(12), 7897–7918. https://doi.org/10.1002/2015jc011012

Chaigneau, A., Gizolme, A., & Grados, C. (2008). Mesoscale eddies off Peru in altimeter records: Identification algorithms and eddy spatiotemporal patterns. *Progress in Oceanography*, *79*(2–4), 106–119. https://doi.org/10.1016/j.pocean.2008.10.013

Chavanne, C. P., & Klein, P. (2010). Can oceanic submesoscale processes be observed with satellite altimetry? *Geophysical Research Letters*, *37*(22), L22602. https://doi.org/10.1029/2010GL045057

Chelton, D. B., Schlax, M. G., & Samelson, R. M. (2011). Global observations of nonlinear mesoscale eddies. *Progress in Oceanography*, *91*(2), 167–216. https://doi.org/10.1016/j.pocean.2011.01.002

Cushman-Roisin, B., Tang, B., & Chassignet, E. P. (1990). Westward motion of mesoscale eddies. *Journal of Physical Oceanography*, *20*(5), 758–768. https://doi.org/10.1175/1520-0485(1990)020<0758:wmome>2.0.co;2

Danilov, S., & Gurarie, D. (2002). Rhines scale and spectra of the β-plane turbulence with bottom drag. *Physical Review* E, *65*(6), 067301. https://doi.org/10.1103/physreve.65.067301

Dee, D. P., Uppala, S. M., Simmons, A. J., Berrisford, P., Poli, P., Kobayashi, S., et al. (2011). The ERA-Interim reanalysis: Configuration and performance of the data assimilation system. *Quarterly Journal of the Royal Meteorological Society*, *137*(656), 553–597. https://doi.org/10.1002/qj.828

Dickson, B., Meincke, J., & Rhines, P. (2008). Arctic–subarctic ocean fluxes: Defining the role of the northern seas in climate. In *Arctic–Subarctic ocean fluxes* (pp. 1–13). Springer.

Dugstad, J. S., Isachsen, P. E., & Fer, I. (2021). The mesoscale eddy field in the Lofoten Basin from high-resolution Lagrangian simulations. *Ocean Science*, *17*(3), 651–674. https://doi.org/10.5194/os-17-651-2021

Dukhovskoy, D., Johnson, M., & Proshutinsky, A. (2006). Arctic decadal variability from an idealized atmosphere-ice-ocean model: 2. Simulation of decadal oscillations. *Journal of Geophysical Research*, *111*(C6), C06029. https://doi.org/10.1029/2004jc002820

Dutkiewicz, S., Rothstein, L., & Rossby, T. (2001). Pathways of cross-frontal exchange in the North Atlantic current. *Journal of Geophysical Research*, *106*(C11), 26917–26928. https://doi.org/10.1029/1999jc000089

Eldevik, T., & Dysthe, K. B. (2002). Spiral eddies. *Journal of Physical Oceanography*, *32*(3), 851–869. https://doi.org/10.1175/1520-0485(2002)032<0851:se>2.0.co;2

Emery, W. J., & Thomson, R. E. (2001). *Data analysis methods in physical oceanography* (Vol. 59, pp. 1–634). Elsevier.

Fahrbach, E. (2006). *ASOF-N: Arctic-Subarctic ocean flux array for European climate: North*. Contract No: EVK2-CT-2002-00139; final report. Arctic-Subarctic Ocean Flux Array for European Climate.

Fairall, C. W., Bradley, E. F., Hare, J. E., Grachev, A. A., & Edson, J. B. (2003). Bulk parameterization of air–sea fluxes: Updates and verification for the COARE algorithm. *Journal of Climate*, *16*(4), 571–591. https://doi.org/10.1175/1520-0442(2003)016<0571:bpoasf>2.0.co;2

Fedorov, A. M., Budyansky, M. V., Belonenko, T. V., Prants, S. V., Uleysky, M. Y., & Bashmachnikov, I. L. (2021). Lagrangian modeling of water circulation in the Lofoten Basin. *Dynamics of Atmospheres and Oceans*, *96*, 101258. https://doi.org/10.1016/j.dynatmoce.2021.101258

Fu, L.-L., & Cazenave, A. (Eds.) (2001)., *Satellite altimetry and earth sciences: A handbook of techniques and applications* (p. 463). Academic Press.

Gascard, J. C., & Mork, K. A. (2008). Climatic importance of large-scale and mesoscale circulation in the Lofoten Basin deduced from Lagrangian observations. In *Arctic–Subarctic ocean fluxes: Defining the role of the northern seas in climate* (pp. 131–143).

Ghaffari, P., Isachsen, P. E., Nøst, O. A., & Weber, J. E. (2018). The influence of topography on the stability of the Norwegian Atlantic Current off northern Norway. *Journal of Physical Oceanography*, *48*(11), 2761–2777. https://doi.org/10.1175/jpo-d-17-0235.1

Good, S. A., Martin, M. J., & Rayner, N. A. (2013). EN4: Quality controlled ocean temperature and salinity profiles and monthly objective analyses with uncertainty estimates. *Journal of Geophysical Research: Oceans*, *118*(12), 6704–6716. https://doi.org/10.1002/2013jc009067

Guinehut, S., Dhomps, A. L., Larnicol, G., & Le Traon, P. Y. (2012). High resolution 3-D temperature and salinity fields derived from in situ and satellite observations. *Ocean Science*, *8*(5), 845–857. https://doi.org/10.5194/os-8-845-2012

Hansen, B., Larsen, K. M. H., Hátún, H., Kristiansen, R., Mortensen, E., & Østerhus, S. (2015). Transport of volume, heat, and salt towards the Arctic in the Faroe current 1993–2013. *Ocean Science*, *11*(5), 743–757. https://doi.org/10.5194/os-11-743-2015

Hansen, B., Østerhus, S., Turrell, W. R., Jónsson, S., Valdimarsson, H., Hátún, H., & Olsen, S. M. (2008). The inflow of Atlantic water, heat, and salt to the Nordic Seas across the Greenland–Scotland ridge. In *Arctic–subarctic ocean fluxes* (pp. 15–43). Springer.

Hattermann, T., Isachsen, P. E., von Appen, W. J., Albretsen, J., & Sundfjord, A. (2016). Eddy-driven recirculation of Atlantic water in Fram Strait. *Geophysical Research Letters*, *43*(7), 1–9. https://doi.org/10.1002/2016GL068323

Hofmann, Z., von Appen, W. J., & Wekerle, C. (2021). Seasonal and mesoscale variability of the two Atlantic Water recirculation pathways in Fram Strait. *Journal of Geophysical Research: Oceans*, *126*(7), e2020JC017057. https://doi.org/10.1029/2020jc017057

Iakovleva, D. A., & Bashmachnikov, I. L. (2021). On the seesaw in interannual variability of upper ocean heat advection between the North Atlantic Subpolar Gyre and the Nordic Seas. *Dynamics of Atmospheres and Oceans*, *96*, 101263. https://doi.org/10.1016/j.dynatmoce.2021.101263

Isachsen, P. E. (2015). Baroclinic instability and the mesoscale eddy field around the Lofoten Basin. *Journal of Geophysical Research: Oceans*, *120*(4), 2884–2903. https://doi.org/10.1002/2014jc010448

Isachsen, P. E., Koszalka, I., & LaCasce, J. H. (2012). Observed and modeled surface eddy heat fluxes in the eastern Nordic Seas. *Journal of Geophysical Research*, *117*(C8), C08020. https://doi.org/10.1029/2012JC007935

Isern-Fontanet, J., García-Ladona, E., & Font, J. (2006). Vortices of the Mediterranean Sea: An altimetric perspective. *Journal of Physical Oceanography*, *36*(1), 87–103. https://doi.org/10.1175/jpo2826.1

Johannessen, J. A., Johannessen, O. M., Svendsen, E., Shuchman, R., Manley, T., Campbell, W. J., et al. (1987). Mesoscale eddies in the Fram Strait marginal ice zone during the 1983 and 1984 marginal ice zone experiments. *Journal of Geophysical Research*, *92*(C7), 6754–6772. https://doi.org/10.1029/jc092ic07p06754

Johannessen, O. M., Johannessen, J. A., Morison, J., Farrelly, B. A., & Svendsen, E. A. S. (1983). Oceanographic conditions in the marginal ice zone north of Svalbard in early fall 1979 with an emphasis on mesoscale processes. *Journal of Geophysical Research*, *88*(C5), 2755–2769. https://doi.org/10.1029/jc088ic05p02755

Kinney, J. C., Maslowski, W., Aksenov, Y., de Cuevas, B., Jakacki, J., Nguyen, A., et al. (2014). On the flow through Bering Strait: A synthesis of model results and observations. In *The Pacific arctic region* (pp. 167–198). Springer.

Kohl, A. (2007). Generation and stability of a quasi-permanent vortex in the Lofoten Basin. *Journal of Physical Oceanography*, *37*(11), 2637–2651. https://doi.org/10.1175/2007jpo3694.1

Kolas, E., & Fer, I. (2018). Hydrography, transport and mixing of the West Spitsbergen current: The Svalbard branch in summer 2015. *Ocean Science*, *14*(6), 1603–1618. https://doi.org/10.5194/os-14-1603-2018

Koszalka, I., LaCasce, J. H., Andersson, M., Orvik, K. A., & Mauritzen, C. (2011). Surface circulation in the Nordic seas from clustered drifters. *Deep-Sea Research, Part 1 58*(4), 468–485. https://doi.org/10.1016/j.dsr.2011.01.007

Kozlov, I. E., Artamonova, A. V., Manucharyan, G. E., & Kubryakov, A. A. (2019). Eddies in the Western Arctic Ocean from spaceborne SAR observations over open ocean and marginal ice zones. *Journal of Geophysical Research: Oceans*, *124*(9), 6601–6616. https://doi.org/10.1029/2019JC015113

Kozlov, I. E., & Atadzhanova, O. A. (2022). Eddies in the marginal ice zone of Fram Strait and Svalbard from spaceborne SAR observations in winter. *Remote Sensing*, *14*(1), 134. https://doi.org/10.3390/rs14010134

Kubryakov, A. A., Kozlov, I. E., & Manucharyan, G. E. (2021). Large mesoscale eddies in the Western Arctic Ocean from satellite altimetry measurements. *Journal of Geophysical Research: Oceans*, *126*(5), e2020JC016670. https://doi.org/10.1029/2020JC016670

Latarius, K., & Quadfasel, D. (2016). Water mass transformation in the deep basins of the Nordic Seas: Analyses of heat and freshwater budgets. *Deep Sea Research Part I: Oceanographic Research Papers*, *114*, 23–42. https://doi.org/10.1016/j.dsr.2016.04.012

Le Traon, P. Y., & Ogor, F. (1998). ERS-1/2 orbit improvement using TOPEX/POSEIDON: The 2 cm challenge. *Journal of Geophysical Research*, *103*(C4), 8045–8057. https://doi.org/10.1029/97jc01917

Ma, C., Guo, X., Zhang, H., Di, J., & Chen, G. (2020). An investigation of the influences of SWOT sampling and errors on ocean eddy observation. *Remote Sensing*, *12*(17), 2682. https://doi.org/10.3390/rs12172682

Morel, Y., & McWilliams, J. (1997). Evolution of isolated interior vortices in the ocean. *Journal of Physical Oceanography*, *27*(5), 727–748. https://doi.org/10.1175/1520-0485(1997)027<0727:eoiivi>2.0.co;2

Mork, K. A., & Skagseth, Ø. (2010). A quantitative description of the Norwegian Atlantic Current by combining altimetry and hydrography. *Ocean Science*, *6*(4), 901–911. https://doi.org/10.5194/os-6-901-2010

Mork, K. A., Skagseth, Ø., & Søiland, H. (2019). Recent warming and freshening of the Norwegian Sea observed by Argo data. *Journal of Climate*, *32*(12), 3695–3705. https://doi.org/10.1175/jcli-d-18-0591.1

Morrow, R., Fu, L. L., Ardhuin, F., Benkiran, M., Chapron, B., Cosme, E., et al. (2019). Global observations of fine-scale ocean surface topography with the Surface Water and Ocean Topography (SWOT) mission. *Frontiers in Marine Science*, *6*, 232. https://doi.org/10.3389/fmars.2019.00232

Nencioli, F., Dong, C., Dickey, T., Washburn, L., & McWilliams, J. C. (2010). A vector geometry-based eddy detection algorithm and its Application to a high-resolution numerical model product and high-frequency radar surface velocities in the Southern California Bight. *Journal of Atmospheric and Oceanic Technology*, *27*(3), 564–579. https://doi.org/10.1175/2009jtecho725.1

Nilsen, F., Gjevik, B., & Schauer, U. (2006). Cooling of the West Spitsbergen current: Isopycnal diffusion by topographic vorticity waves. *Journal of Geophysical Research*, *111*(C8), C08012. https://doi.org/10.1029/2005jc002991

Nurser, A. J. G., & Bacon, S. (2014). The Rossby radius in the Arctic Ocean. *Ocean Science*, *10*(6), 967–975. https://doi.org/10.5194/os-10-967-2014

Orvik, K. A., & Niiler, P. (2002). Major pathways of Atlantic water in the northern North Atlantic and Nordic seas toward Arctic. *Geophysical Research Letters*, *29*(19), 2-1–2–4. https://doi.org/10.1029/2002gl015002

Paillet, J., Le Cann, B., Carton, X., Morel, Y., & Serpette, A. (2002). Dynamics and evolution of a northern meddy. *Journal of Physical Oceanography*, *32*(1), 55–79. https://doi.org/10.1175/1520-0485(2002)032<0055:daeoan>2.0.co;2

Raj, R. P., Chafik, L., Nilsen, J. E. Ø., Eldevik, T., & Halo, I. (2015). The Lofoten vortex of the Nordic seas. *Deep Sea Research Part I: Oceanographic Research Papers*, *96*, 1–14. https://doi.org/10.1016/j.dsr.2014.10.011

Raj, R. P., & Halo, I. (2016). Monitoring the mesoscale eddies of the Lofoten Basin: Importance, progress, and challenges. *International Journal of Remote Sensing*, *37*(16), 3712–3728. https://doi.org/10.1080/01431161.2016.1201234

Raj, R. P., Halo, I., Chatterjee, S., Belonenko, T., Bakhoday-Paskyabi, M., Bashmachnikov, I., et al. (2020). Interaction between mesoscale eddies and the gyre circulation in the Lofoten Basin. *Journal of Geophysical Research: Oceans*, *125*(7), e2020JC016102. https://doi.org/10.1029/2020jc016102

Raj, R. P., Johannessen, J. A., Eldevik, T., Nilsen, J. E. Ø., & Halo, I. (2016). Quantifying mesoscale eddies of the Lofoten Basin. *Journal of Geophysical Research: Oceans*, *121*(7), 4503–4521. https://doi.org/10.1002/2016JC011637

Raj, R. P., Nilsen, J. Ø., Johannessen, J. A., Furevik, T., Andersen, O. B., & Bertino, L. (2018). Quantifying Atlantic water transport to the Nordic seas by remote sensing. *Remote Sensing of Environment*, *216*, 758–769. https://doi.org/10.1016/j.rse.2018.04.055

Richards, C. G., & Straneo, F. (2015). Observations of water mass transformation and eddies in the Lofoten Basin of the Nordic seas. *Journal of Physical Oceanography*, *45*(6), 1735–1756. https://doi.org/10.1175/jpo-d-14-0238.1

Rossby, T., Ozhigin, V., Ivshin, V., & Bacon, S. (2009). An isopycnal view of the Nordic Seas hydrography with focus on properties of the Lofoten Basin. *Deep Sea Research Part I: Oceanographic Research Papers*, *56*(11), 1955–1971. https://doi.org/10.1016/j.dsr.2009.07.005

Rudels, B. (2015). Arctic Ocean circulation, processes and water masses: A description of observations and ideas with focus on the period prior to the international polar year 2007–2009. *Progress in Oceanography*, *132*, 22–67. https://doi.org/10.1016/j.pocean.2013.11.006

Sandven, S., Johannessen, O. M., & Johannessen, J. A. (1991). Mesoscale eddies and chimneys in the marginal ice zone. *Journal of Marine Systems*, *2*(1–2), 195–208. https://doi.org/10.1016/0924-7963(91)90024-o

Schauer, U., & Beszczynska-Möller, A. (2009). Problems with estimation and interpretation of oceanic heat transport–conceptual remarks for the case of Fram Strait in the Arctic Ocean. *Ocean Science*, *5*(4), 487–494. https://doi.org/10.5194/os-5-487-2009

Schauer, U., Beszczynska-Möller, A., Walczowski, W., Fahrbach, E., Piechura, J., & Hansen, E. (2008). Variation of measured heat flow through the Fram Strait between 1997 and 2006. In *Arctic–Subarctic ocean fluxes* (pp. 65–85). Springer.

Schauer, U., Fahrbach, E., Osterhus, S., & Rohardt, G. (2004). Arctic warming through the Fram Strait: Oceanic heat transport from 3 years of measurements. *Journal of Geophysical Research*, *109*(C6), C06026. https://doi.org/10.1029/2003jc001823

Shapiro, G. I., & Meschanov, S. L. (1996). Spreading pattern and mesoscale structure of Mediterranean outflow in the Iberian Basin estimated from historical data. *Journal of Marine Systems*, *7*(2–4), 337–348. https://doi.org/10.1016/0924-7963(95)00011-9

Skagseth, Ø. (2008). Recirculation of Atlantic water in the western Barents Sea. *Geophysical Research Letters*, *35*(11), L11606. https://doi.org/10.1029/2008GL033785

Skagseth, Ø., Drinkwater, K. F., Drinkwater, K. F., & Terrile, E. (2011). Wind-and buoyancy-induced transport of the Norwegian coastal current in the Barents Sea. *Journal of Geophysical Research*, *116*(C8), C08007. https://doi.org/10.1029/2011jc006996

Skagseth, Ø., Furevik, T., Ingvaldsen, R., Loeng, H., Mork, K. A., Orvik, K. A., & Ozhigin, V. (2008). Volume and heat transports to the Arctic Ocean via the Norwegian and Barents seas. In *Arctic–Subarctic ocean fluxes* (pp. 45–64). Springer.

Smedsrud, L. H., Esau, I., Ingvaldsen, R. B., Eldevik, T., Haugan, P. M., Li, C., et al. (2013). The role of the Barents Sea in the Arctic climate system. *Reviews of Geophysics*, *51*(3), 415–449. https://doi.org/10.1002/rog.20017

Smedsrud, L. H., Ingvaldsen, R., Nilsen, J. Ø., & Skagseth, Ø. (2010). Heat in the Barents Sea: Transport, storage, and surface fluxes. *Ocean Science*, *6*(1), 219–234. https://doi.org/10.5194/osd-6-1437-2009

Smedsrud, L. H., Muilwijk, M., Brakstad, A., Madonna, E., Lauvset, S. K., Spensberger, C., et al. (2022). Nordic Seas heat loss, Atlantic inflow, and Arctic sea ice cover over the last century. *Reviews of Geophysics*, *60*(1), e2020RG000725. https://doi.org/10.1029/2020rg000725

Spall, M. A. (2010). Dynamics of downwelling in an eddy-resolving convective basin. *Journal of Physical Oceanography*, *40*(10), 2341–2347. https://doi.org/10.1175/2010jpo4465.1

Spall, M. A., Almansi, M., Huang, J., Haine, T. W., & Pickart, R. S. (2021). Lateral redistribution of heat and salt in the Nordic Seas. *Progress in Oceanography*, *196*, 102609. https://doi.org/10.1016/j.pocean.2021.102609

Spall, M. A., & Chapman, D. C. (1998). On the efficiency of baroclinic eddy heat transport across narrow fronts. *Journal of Physical Oceanography*, *28*(11), 2275–2287. https://doi.org/10.1175/1520-0485(1998)028<2275:oteobe>2.0.co;2

Stammer, D. (2005). Adjusting internal model errors through ocean state estimation. *Journal of Physical Oceanography*, *35*(6), 1143–1153. https://doi.org/10.1175/jpo2733.1

Taburet, G., Sanchez-Roman, A., Ballarotta, M., Pujol, M. I., Legeais, J. F., Fournier, F., et al. (2019). DUACS DT2018: 25 years of reprocessed sea level altimetry products. *Ocean Science*, *15*(5), 1207–1224. https://doi.org/10.5194/os-15-1207-2019

Treguier, A. M., Mathiot, P., Graham, T., Copsey, D., Lique, C., & Sterlin, J. (2021). Heat balance in the Nordic Seas in a global 1/12° coupled model. *Journal of Climate*, *34*(1), 89–106. https://doi.org/10.1175/jcli-d-20-0063.1

Trodahl, M., & Isachsen, P. E. (2018). Topographic influence on baroclinic instability and the mesoscale eddy field in the northern North Atlantic Ocean and the Nordic Seas. *Journal of Physical Oceanography*, *48*(11), 2593–2607. https://doi.org/10.1175/jpo-d-17-0220.1

Trodahl, M., Isachsen, P. E., Lilly, J. M., Nilsson, J., & Kristensen, N. M. (2020). The regeneration of the Lofoten Vortex through vertical alignment. *Journal of Physical Oceanography*, *50*(9), 2689–2711. https://doi.org/10.1175/jpo-d-20-0029.1

Verbrugge, N., Mulet, S., Guinehut, S., & Buongiorno-Nardelli, B. (2017). ARMOR3D: A 3D multi-observations T,S,U,V product of the ocean. In *19th EGU genernal assembly EGU2017, proceedings from conf. held 23–28 April. 2017 Vienna, Austria* (Vol. 19, p. 17579).

Vesman, A. V. (2021). Features of the manifestation of global warming in the XX-XXI centuries in the waters washing the archipelago Spitzbergen. PhD thesis, see the English version of the thesis following the one in Russian in the document Dissertation. St.Petergbur State University. defended 03.06.2022 Retrieved from https://disser.spbu.ru/zashchita-uchenoj-stepeni-spbgu/606-vesman-anna-viktorovna/

Volkov, D. L., Kubryakov, A. A., & Lumpkin, R. (2015). Formation and variability of the Lofoten basin vortex in a high-resolution ocean model. *Deep Sea Research Part I: Oceanographic Research Papers*, *105*, 142–157. https://doi.org/10.1016/j.dsr.2015.09.001

Volkov, D. L., & Pujol, M. I. (2012). Quality assessment of a satellite altimetry data product in the Nordic, Barents, and Kara seas. *Journal of Geophysical Research*, *117*(C3), C03025. https://doi.org/10.1029/2011jc007557

von Appen, W. J., Schauer, U., Somavilla, R., Bauerfeind, E., & Beszczynska-Möller, A. (2015). Exchange of warming deep waters across Fram Strait. *Deep Sea Research Part I: Oceanographic Research Papers*, *103*, 86–100. https://doi.org/10.1016/j.dsr.2015.06.003

von Appen, W. J., Wekerle, C., Hehemann, L., Schourup-Kristensen, V., Konrad, C., & Iversen, M. H. (2018). Observations of a submesoscale cyclonic filament in the marginal ice zone. *Geophysical Research Letters*, *45*(12), 6141–6149. https://doi.org/10.1029/2018GL077897

von Appen, W. J. V., Schauer, U., Hattermann, T., & Beszczynska-Möller, A. (2016). Seasonal cycle of mesoscale instability of the West Spitsbergen current. *Journal of Physical Oceanography*, *46*(4), 1231–1254. https://doi.org/10.1175/jpo-d-15-0184.1

Walczowski, W. (2014). Atlantic water in the Nordic seas. Properties, variability, climatic significance. In *GeoPlanet: Earth and planetary sciences* (pp. 1–174). Springer. https://doi.org/10.1007/978-3-319-01279-7

Wang, Q., Koldunov, N. V., Danilov, S., Sidorenko, D., Werkerle, C., Scholz, P., et al. (2020). Eddy kinetic energy in the Arctic Ocean from a global simulation with a 1-km Arctic. *Geophysical Research Letters*, *47*(14), e2020GL088550. https://doi.org/10.1029/2020GL088550

Wekerle, C., Hattermann, T., Wang, Q., Crews, L., von Appen, W. J., & Danilov, S. (2020). Properties and dynamics of mesoscale eddies in Fram Strait from a comparison between two high-resolution ocean–sea ice models. *Ocean Science*, *16*(5), 1225–1246. https://doi.org/10.5194/os-16-1225-2020

Yu, L. S., Bosse, A., Fer, I., Orvik, K. A., Bruvik, E. M., Hessevik, I., & Kvalsund, K. (2017). The Lofoten Basin eddy: Three years of evolution as observed by Seagliders. *Journal of Geophysical Research: Oceans*, *122*(8), 6814–6834. https://doi.org/10.1002/2017jc012982

Zhurbas, V., Väli, G., & Kuzmina, N. (2019). Rotation of floating particles in submesoscale cyclonic and anticyclonic eddies: A model study for the southeastern Baltic Sea. *Ocean Science*, *15*(6), 1691–1705. https://doi.org/10.5194/os-15-1691-2019